Wave Motion 107 (2021) 102822

Contents lists available at ScienceDirect

Wave Motion

journal homepage: www.elsevier.com/locate/wamot

Solution of three-dimensional multiple scattering problems by the method of difference potentials☆

M. Medvinsky [a], S. Tsynkov [a,*], E. Turkel [b]

[a] Department of Mathematics, North Carolina State University, Box 8205, Raleigh, NC 27695, USA
[b] School of Mathematical Sciences, Tel Aviv University, Ramat Aviv, Tel Aviv 69978, Israel

ARTICLE INFO

Article history:
Received 10 August 2020
Received in revised form 8 June 2021
Accepted 23 August 2021
Available online 30 August 2021

Keywords:
Time-harmonic waves
Unbounded domain
Helmholtz equation
Finite differences
High-order accuracy
Scattering objects
Cartesian grid
Non-conforming boundary
Artificial outer boundary
BGT radiation condition

ABSTRACT

We propose an algorithm based on the Method of Difference Potentials (MDP) for the numerical solution of multiple scattering problems in three space dimensions. The propagation of waves is assumed time-harmonic and governed by the Helmholtz equation. The latter is approximated with 6th order accuracy on a Cartesian grid by means of a compact finite difference scheme. The shape of the scatterers does not have to conform to the discretization grid, yet the MDP enables the approximation with no loss of accuracy. At the artificial outer boundary, which is spherical, the solution is terminated by a 6th order Bayliss–Gunzburger–Turkel (BGT) radiation boundary condition. The method enables efficient solution of a series of similar problems, for example, when the incident field changes while everything else stays the same, or when the type of the scattering changes (e.g., sound-soft vs. sound-hard) while the shape of the scatterer remains the same.

1. Introduction

In this paper, we consider the computation of single-frequency wave scattering about multiple bodies in three-dimensional space (see Fig. 1). Such problems appear in several physical connections including electrodynamics [1] and photonics [2,3], especially in periodic media [4,5], see Martin [6] for further information. Because of interactions between the scatterers, complex structures can appear in the field. This creates several computational difficulties. First, one may require a fine mesh to resolve these complex structures. Furthermore, in many applications the scatterers sit in an unbounded medium, which computationally requires an artificial boundary condition. Again, because of the interaction between the bodies the artificial outer boundary may need to be relatively far from the bodies. Finally, if the bodies are highly separated a large grid is required. One approach is to use an integral equation formulation [6–9]. It results in large nonlocal matrices to invert and hence requires a very large computer memory. Even fast multipole methods are still very expensive especially in three dimensions. Hence, we will consider a field approach and employ a sixth order accurate compact finite difference scheme [10]. This scheme enables us to use a coarser grid for a similar accuracy which is of

☆ Work supported by the US Army Research Office (ARO) under grant # W911NF-16-1-0115, and by the US–Israel Binational Science Foundation (BSF), Israel under grant # 2014048.

* Corresponding author.
E-mail addresses: mmedvin@ncsu.edu (M. Medvinsky), tsynkov@math.ncsu.edu (S. Tsynkov), turkel@tauex.tau.ac.il (E. Turkel).
URLs: https://mmedvin.math.ncsu.edu (M. Medvinsky), https://stsynkov.math.ncsu.edu (S. Tsynkov), https://www.math.tau.ac.il/~turkel (E. Turkel).

https://doi.org/10.1016/j.wavemoti.2021.102822
0165-2125/

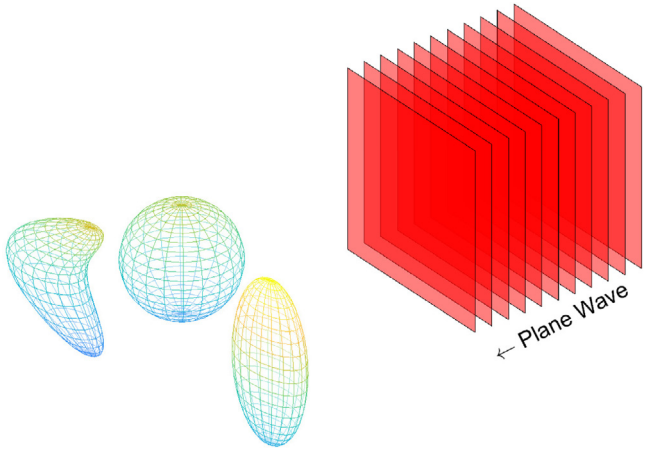

Fig. 1. Multiple scatterers in space illuminated by a plane wave.

utmost importance in three dimensions and especially for a problem with several bodies. Furthermore, the density of the grid grows almost linearly, i.e., it scales as $k^{7/6}$, where k is the spatial frequency (wavenumber), in contrast to lower order methods where the pollution effect demands that the grid grow considerably faster than linear with the frequency. To account for the general shaped obstacles, we use the method of difference potentials (MDP) [11]. When combined with scheme [10], the MDP allows us to achieve high order accuracy for non-conforming boundaries while still using only simple structured grids such as Cartesian or spherical. Thus, the solution of the resultant linear system is efficient.

Our approach has several advantages compared to finite elements. First, it does not require any grid generation because the MDP guarantees high order accuracy for non-conforming shapes, while the construction of a finite element curvilinear grid about several bodies is nontrivial. In addition, our discretization [10] attains sixth order accuracy economically as it keeps the number of unknowns to a minimum — one per grid node. In contrast, a high order finite element method requires additional degrees of freedom and thus the linear system to be solved appears more difficult.

The problem we are solving is formulated on an unbounded region. There are two basic approaches to obtaining a finite difference or finite element solution for multiple scattering in this case. The first approach is to construct an artificial surface surrounding all the bodies and to solve the Helmholtz equation over the entire region with some artificial boundary condition (ABC). This has the disadvantage that one grid needs to be constructed for all the obstacles which can be expensive especially if the bodies are spaced far apart. Another approach which has been developed over the past few years is to surround each obstacle with its own ABC achieving a domain decomposition of the total problem. This assumes that the various bodies are far enough apart so that one can construct non-intersecting spheres (circles) about each body. The ABC for each obstacle must allow outgoing waves from that obstacle without reflections but allow incoming waves from the other obstacles. Grote and Kirsch [12] developed such an approach using DtN as the nonreflecting boundary condition coupled with a second order finite difference scheme in polar coordinates for each scatterer. A key component of work [12] is the propagation and transfer operators that supply the incoming field to a given artificial boundary from all other boundaries. It is these operators that render connections between individual subdomains across the white space that is not covered with the grid. They are constructed analytically using the Fourier–Hankel expansions. The resulting solution is compared in [12] against a second order finite element solution inside one artificial boundary surrounding all scatterers. Additional similar approaches using a DtN map have been developed by Acosta and Villamizar [13] and by Min and Kim [14] who considered scattering in waveguides. Jiang and Zheng [15] used a domain decomposition with termination by a perfectly matched layer (PML) and a second order Lagrange finite element code. The domain is Cartesian and the obstacles are either cubes or L-shaped, which align with the grid. A similar approach is to use absorbing boundary conditions directly on the scatterers — the so-called on-surface radiation conditions (OSRC), see, e.g., [16–18].

An extension of [12] to the time-dependent wave equation was later developed by Grote and Sim [19] using a local ABC for multiple obstacles. The local ABC is that of Bayliss and Turkel (BT) [20] as reconstructed by Hagstrom and Hariharan [21]. This expresses each term of the BT formula via a new auxiliary equation that involves a time derivative and a Laplacian along the outer sphere (Laplace–Beltrami operator in spherical coordinates). Grote and Sim then develop a solution in terms of spherical harmonics. Similarly to the propagation and transfer operators of [12], it is used to provide the incoming wave due to the contributions of the other obstacles. In practice, they use a second order finite difference scheme to solve the wave equation. They consider the case where the obstacles are spheres and use spherical coordinates about each separate obstacle.

In this study, we revert to the first approach and solve a single-frequency multiple scattering problem for the entire domain containing all the obstacles. As opposed to a finite element approach of [12], we use only a Cartesian grid and so have no need to construct a grid that matches the embedded obstacles. Though our examples are spheres, they do not

align with the Cartesian grid and a more general shape can be accommodated as well. Also as opposed to the previously mentioned techniques, we use a sixth order accurate scheme (rather than second order scheme) and hence can use a coarser grid to resolve the complex physics. Moreover, with the appropriate modifications to the finite difference scheme our approach can handle the variable speed of sound, while the propagation and transfer operators needed in the case of separate ABCs set for each individual scatterer require that the speed of sound be constant.

To account for the unbounded domain, we introduce a local absorbing boundary condition. In particular, we use that of Bayliss–Gunzburger–Turkel (BGT) [22]. Because of the need to reduce the grid domain and also the complex solution, we use a sixth order BGT condition at the artificial outer surface. In its original formulation, the BGT condition is difficult to implement beyond the second order term. Hence, we shall use a reformulation given in [23] that easily allows higher order terms of BGT in spherical coordinates. Thus, we combine a sixth order compact interior scheme with a sixth order BGT operator at the outer boundary. Our choice of a local high order ABC rather than a PML at the artificial outer boundary is motivated by the accuracy considerations. In the case of a PML, to attain the overall sixth order accuracy one must discretize with sixth order accuracy not only the Helmholtz equation inside the computational domain but also the more complicated governing equations inside the layer. The use of an ABC helps us avoid that.

The use of a high order BGT allows us to bring the outer artificial surface closer in. Since we are solving on the entire 3D domain that surrounds all the scatterers, the required memory use is still substantial. This, however, is compensated for by the versatility of the MDP. In particular, our code works with any boundary conditions on the obstacles, such as soft, hard, Robin, or other, including different types on different scatterers. In doing so, the additional computational cost for accommodating a different boundary condition (or a different incident field) is very small, provided that the scattering geometry does not change so that the discrete Calderon's operators in the framework of MDP can be computed once ahead of time. If desired, one can also use the approach of Grote and Sim [19] (translated to the frequency space) and replace their version of BT via Hagstrom–Hariharan [21] by our direct implementation of any higher order BGT in spherical harmonics [23]. On the other hand, our approach that involves a sixth order BGT can also be modified so that to solve only inside separate artificial boundaries surrounding individual scatterers. The MDP will still be used to allow for non-conforming surfaces on regular grids and to account for various types of scattering surfaces, while transmission operators based on spherical-Hankel expansions (similar to those of [12]) will be needed to transfer the information between different subdomains. This modification will be developed in the future.

To summarize, there are three main components of the proposed methodology: a sixth order accurate compact scheme [10], the method of difference potentials [11], and a high order BGT boundary condition [23]. The key novel contribution of the current paper is that these three components are brought together to efficiently solve a class of challenging three-dimensional problems that appear in a variety of applications. Note that in [24], we have solved some two-dimensional multiple scattering problems that involved layered structures, but multiple scattering about disjoint bodies in three space dimensions has not been addressed in any of our previous work.

In Section 2, we formulate a 3D multiple scattering problem, followed by the solution based on the method of difference potentials [11] in Section 3, and the numerical experiments in Section 4.

2. Multiple scattering problem

We consider the scattering of a scalar monochromatic field about multiple smooth disjoint objects Ω_q in $\boldsymbol{R}^3$, $q = 1, \ldots, N$. The scatterers Ω_q may have arbitrary shape, although in the specific examples we analyze in the current work all scatterers are spherical (see Fig. 2). In the frequency domain, the propagation of waves is governed by the Helmholtz equation:

$$Lu \equiv \Delta u + k^2 u = 0. \tag{1}$$

Eq. (1) is to be solved on $\boldsymbol{R}^3 \backslash S_N$, where $S_N = \bigcup_{q=1}^{N} \Omega_q$ is the union of all scatterers.

The problem is driven by the incident field $u^{(inc)}$, which can be a plane wave with wavenumber k propagating at a given direction (specified by the angles ϑ and ϕ):

$$u^{(inc)} = e^{ik(x\cos\vartheta\sin\phi + y\sin\vartheta\sin\phi + z\cos\phi)}. \tag{2}$$

Alternatively, one can choose the incident field to be a spherical wave originating at $\boldsymbol{x}_0 \notin S_N$:

$$u^{(inc)}(\boldsymbol{x}) = \frac{e^{ik(\|\boldsymbol{x}-\boldsymbol{x}_0\|)}}{\|\boldsymbol{x}-\boldsymbol{x}_0\|}. \tag{3}$$

The overall solution u is the sum of the incident and scattered components: $u(\boldsymbol{x}) = u^{(inc)}(\boldsymbol{x}) + u^{(scat)}(\boldsymbol{x})$. It requires a boundary condition on $\partial S_N = \bigcup_{q=1}^{N} \Gamma_q$, where $\Gamma_q = \partial\Omega_q$. For each individual Γ_q, $q = 1, \ldots, N$, the type of the boundary condition, which is determined by the type of scattering, can be different.[1] For soft scattering, $u = 0$ at the boundary, which yields a Dirichlet boundary condition for the scattered field: $u^{(scat)}\big|_{\Gamma_q} = -u^{(inc)}\big|_{\Gamma_q}$. For hard scattering, the normal derivative is zero at the boundary, $\frac{\partial u}{\partial \boldsymbol{n}} = 0$, and a Neumann boundary transpires: $\frac{\partial u^{(scat)}}{\partial \boldsymbol{n}}\big|_{\Gamma_q} = -\frac{\partial u^{(inc)}}{\partial \boldsymbol{n}}\big|_{\Gamma_q}$. Robin (impedance)

[1] One can have different types of scattering even on different parts of one and the same Γ_q.

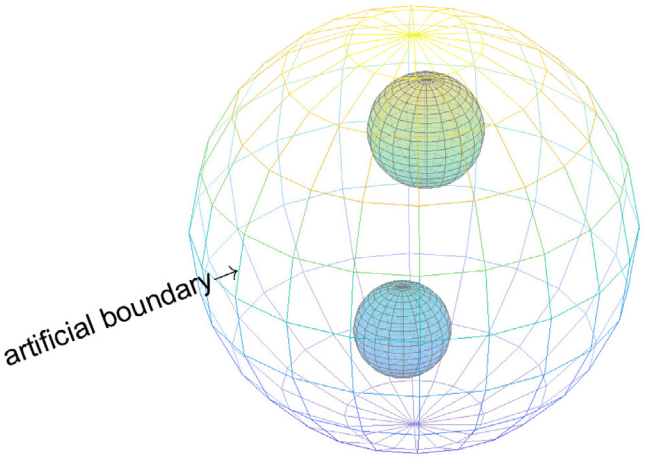

Fig. 2. Two spherical scatterers surrounded by a spherical artificial boundary.

boundary condition can be considered as well. To ensure uniqueness of the solution u, the scattered field $u^{(scat)}$ should satisfy the Sommerfeld radiation condition at infinity:

$$\frac{\partial u^{(scat)}(\boldsymbol{x})}{\partial |\boldsymbol{x}|} - iku^{(scat)}(\boldsymbol{x}) = o\left(\frac{1}{|\boldsymbol{x}|}\right) \quad \text{as} \quad |\boldsymbol{x}| \to \infty. \tag{4}$$

2.1. Truncation of the unbounded domain

In order to solve the problem (1)–(4) numerically, one truncates the original unbounded domain and introduces an artificial outer boundary. In our case, the outer boundary is a sphere of radius R_0 (see Fig. 2) and the computational domain is the ball

$$\Omega_0 = \{(r, \theta, \varphi) | r \leqslant R_0,\ 0 \leqslant \theta \leqslant \pi,\ 0 \leqslant \varphi < 2\pi\}. \tag{5}$$

We require that $S_N \subset \Omega_0$. To approximate the Sommerfeld condition (4) on the sphere $\Gamma_0 \equiv \partial\Omega_0$, we employ a 6th order Bayliss–Gunzburger–Turkel (BGT) ABC [22,23].

The BGT radiation conditions [22] are given in the form

$$B_m u\big|_{r=R_0} = 0, \tag{6}$$

where the operators B_m are defined by the following recursive relations starting from $B_0 = I$:

$$B_m u = \left(\frac{\partial}{\partial r} - ik + \frac{2m-1}{r}\right) B_{m-1} u, \quad m = 2, 3, \ldots \tag{7}$$

In our previous work [23], we replaced (7) with

$$B_m u = \alpha_m \frac{\partial u}{\partial r} + \sum_{n=1}^{\lfloor \frac{m}{2} \rfloor} \beta_{m,n} \Delta_{\theta,\varphi}^n u + \sum_{n=1}^{\lfloor \frac{m-1}{2} \rfloor} \gamma_{m,n} \Delta_{\theta,\varphi}^n \frac{\partial u}{\partial r} + \left(\frac{1}{r} - ik\right) \alpha_m u, \tag{8}$$

where $\Delta_{\theta,\varphi}$ is the Beltrami operator on the sphere (i.e., spherical part of the 3D Laplacian):

$$\Delta_{\theta,\varphi} u = \frac{1}{\sin\theta} \frac{\partial}{\partial\theta}\left(\sin\theta \frac{\partial u}{\partial\theta}\right) + \frac{1}{\sin^2\varphi} \frac{\partial^2 u}{\partial\varphi^2}, \tag{9}$$

and the coefficients are defined recursively:

$$\alpha_m = \left(1 + \frac{2}{r}(m - ikr - 1)\right) \alpha_{m-1},$$

$$\beta_{m,1} = \left(1 + \frac{1}{r}(2m - ikr - 1)\right) \beta_{m-1,1} - \gamma_{m-1,1} k^2 - \frac{\alpha_{m-1}}{r^2},$$

$$\beta_{m,n} = \left(1 + \frac{1}{r}(2m - ikr - 1)\right) \beta_{m-1,n} - \gamma_{m-1,n} k^2 - \frac{\gamma_{m-1,n-1}}{r^2}, \quad n > 1,$$

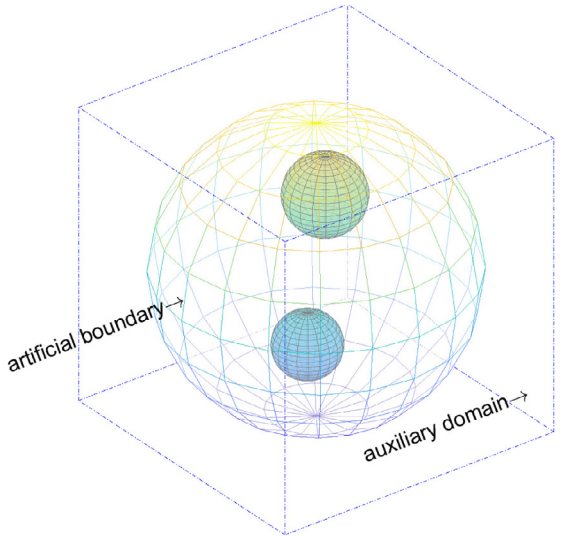

Fig. 3. Scatterers surrounded by artificial outer boundary inside the cubical auxiliary domain.

$$\gamma_{m,n} = \left(1 + \frac{1}{r}\,(2m - ikr - 3)\right)\gamma_{m-1,n} + \beta_{m-1,n},$$

subject to the initial conditions at $m = 1$: $\alpha_1 = 1$ and $\forall n:\ \beta_{1,n} = \gamma_{1,n} = 0$. The 6th order BGT used in the current work is given explicitly by

$$\begin{aligned} B_6 u = &\left(\frac{18}{r^5} - \frac{6ik}{r^4}\right)\Delta^2_{\theta,\varphi}\frac{\partial u}{\partial r} + \left(-\frac{32ik^3}{r^2} + \frac{288k^2}{r^3} + \frac{708ik}{r^4} - \frac{444}{r^5}\right)\Delta_{\theta,\varphi}\frac{\partial u}{\partial r} \\ &+ \left(-32ik^5 + \frac{480k^4}{r} + \frac{2400ik^3}{r^2} - \frac{4800k^2}{r^3} - \frac{3600ik}{r^4} + \frac{720}{r^5}\right)\frac{\partial u}{\partial r} - \frac{1}{r^6}\Delta^3_{\theta,\varphi}u \\ &+ \left(-\frac{18k^2}{r^4} - \frac{108ik}{r^5} + \frac{136}{r^6}\right)\Delta^2_{\theta,\varphi}u \\ &+ \left(-\frac{48k^4}{r^2} - \frac{544ik^3}{r^3} + \frac{1980k^2}{r^4} + \frac{2664ik}{r^5} - \frac{1044}{r^6}\right)\Delta_{\theta,\varphi}u \\ &+ \left(-32k^6 - \frac{512ik^5}{r} + \frac{2880k^4}{r^2} + \frac{7200ik^3}{r^3} - \frac{8400k^2}{r^4} - \frac{4320ik}{r^5} + \frac{720}{r^6}\right)u. \end{aligned} \tag{10}$$

We emphasize that the BGT radiation condition (6) with sixth order operator B_6 of (10) still contains no radial derivatives higher than first order; all high order derivatives contained in the Laplace–Beltrami operator $\Delta_{\theta,\varphi}$ and its powers are tangential. Therefore, we do not expect any issues with well-posedness when this boundary condition is applied to the Helmholtz equation, which is a second order elliptic PDE. The results of our computations reported in [23], as well as in Section 4 of this paper, corroborate these expectations.

3. Solution by the method of difference potentials

We are interested in solving equation (1) on the domain $\Omega = \Omega_0 \setminus S_N$. Using the method of difference potentials (MDP) [11], we reduce it to a system of operator equations on the boundaries Γ_q and $\partial\Omega_0$ that involves discrete counterparts to Calderon's projections [25,26]. The discrete Calderon's projections are computed with the help of a sixth order accurate compact finite difference scheme on a simple Cartesian grid. The boundary conditions on Γ_q, $q = 1, \ldots, N$, as well as the BGT radiation condition (6), (10) on the sphere $\partial\Omega_0$, are efficiently implemented in the framework of MDP without having to approximate them on the grid.

3.1. Auxiliary problem

Consider an auxiliary domain $\widetilde{\Omega} \supset \Omega_0$ shaped as a cube with side $2R_1$, $R_1 > R_0$ (see Fig. 3):

$$\widetilde{\Omega} = [-R_1, R_1] \times [-R_1, R_1] \times [-R_1, R_1]. \tag{11}$$

Let $\mathbb{N}$ be a uniform Cartesian grid on $\widetilde{\Omega}$:

$$\mathbb{N} = \left\{ (x_s, y_t, z_p) \;\middle|\; \begin{array}{ll} x_s = sh_x, & s = 0, \ldots, S \\ y_t = th_y, & t = 0, \ldots, T \\ z_p = ph_z, & p = 0, \ldots, P \end{array} \right\}. \tag{12}$$

Similarly, let $\mathbb{M} \subset \mathbb{N}$ be another Cartesian grid on $\widetilde{\Omega}$ that does not include the outermost nodes of $\mathbb{N}$ on the surface of the cube (11):

$$\mathbb{M} = \left\{ (x_s, y_t, z_p) \;\middle|\; \begin{array}{ll} x_s = sh_x, & s = 1, \ldots, S-1 \\ y_t = th_y, & t = 1, \ldots, T-1 \\ z_p = ph_z, & p = 1, \ldots, P-1 \end{array} \right\}. \tag{13}$$

For simplicity, and with no loss of generality, we will assume that $h_x = h_y = h_z = h$ hereafter so that $T = P = S$. We approximate the Helmholtz equation (1) using a 6th order accurate compact equation-based finite difference scheme [27]:

$$\boldsymbol{L}^{(h)} u^{(h)} = 0, \tag{14}$$

where $u^{(h)}$ is the discrete solution of the Helmholtz equation on the grid $\mathbb{N}$ of (12). In the interior nodes $\mathbb{M} \subset \mathbb{N}$, the operator $\boldsymbol{L}^{(h)}$ on the left-hand side of (14) is defined as follows:

$$\begin{aligned} \boldsymbol{L}^{(h)} u^{(h)}\Big|_{(s,t,p)\in\mathbb{M}} = {} & \left(D_{xx} + D_{yy} + D_{zz}\right)\left(1 + \frac{k^2h^2}{30}\right) u^{(h)} + \frac{h^4}{30} D_{xx}D_{yy}D_{zz} u^{(h)} \\ & + \left(1 - \frac{k^2h^2}{20}\right) k^2 u^{(h)} + \frac{h^2}{6}\left(D_{xx}D_{yy} + D_{xx}D_{zz} + D_{yy}D_{zz}\right)\left(1 + \frac{k^2h^2}{15}\right) u^{(h)}, \end{aligned} \tag{15}$$

where

$$D_{xx} u^{(h)} = \frac{u_{s+1,t,p} - 2u_{s,t,p} + u_{s-1,t,p}}{h^2}$$

and similarly for the coordinate directions y and z. The finite difference Eqs. (14), (15) are supplemented by the boundary conditions on the exterior surface $\mathbb{N}\backslash\mathbb{M}$ of the grid $\mathbb{N}$. Specifically, in the coordinate directions y and z we set:

$$u^{(h)}\Big|_{t=0} = u^{(h)}\Big|_{t=S} = u^{(h)}\Big|_{p=0} = u^{(h)}\Big|_{p=S} = 0, \tag{16}$$

i.e., the solution is required to satisfy the zero Dirichlet boundary conditions at $y = \pm R_1$ and $z = \pm R_1$, see (11). In the coordinate direction x, we set the complex impedance boundary conditions

$$\begin{aligned} & u_x + iku = 0, \quad x = R_1, \\ & u_x - iku = 0, \quad x = -R_1. \end{aligned} \tag{17}$$

Boundary conditions (17) are also commonly referred to as Sommerfeld-type radiation conditions (see, e.g., [28, Chapter VII, Section 3] or [29, Chapter 9, Section 9.3]). They guarantee uniqueness of the solution to the Helmholtz equation because they shift the spectrum of the problem to the complex plane and as such, $-k^2$ for $k \in \mathbb{R}$ may no longer be an eigenvalue of the Laplacian. The discrete boundary conditions in the coordinate direction x approximate boundary conditions (17) with sixth order accuracy [27, Section 3]:

$$\begin{aligned} & \frac{u_{S+1,t,p} + 2ikh\left(1 - \frac{k^2h^2}{6} + \frac{k^4h^4}{120}\right) u_{S,t,p} - u_{S-1,t,p}}{2h} = 0, \\ & \frac{u_{1,t,p} + 2ikh\left(1 - \frac{k^2h^2}{6} + \frac{k^4h^4}{120}\right) u_{0,t,p} - u_{-1,t,p}}{2h} = 0. \end{aligned} \tag{18}$$

The ghost nodes $(S+1, t, p)$ and $(-1, t, p)$ are eliminated from (18) by formally extending the finite difference approximation (14), (15) of the Helmholtz equation (1) all the way up to the boundaries $x = \pm R_1$, i.e., to the nodes (S, t, p) and $(0, t, p)$. The resulting overall system of linear finite difference Eqs. (14), (15), (16), (18) has only the trivial solution, because the complex impedance boundary conditions (17) prevent resonances at real frequencies k. Consequently, the inhomogeneous finite difference equation [cf. equation (14)]

$$\boldsymbol{L}^{(h)} u^{(h)} = g^{(h)}, \tag{19}$$

subject to boundary conditions (16), (18) has a unique solution $u^{(h)}$ on the grid $\mathbb{N}$ of (12) for any right-hand side $g^{(h)}$ defined on the grid $\mathbb{M}$ of (13). Henceforth, the system of finite difference Eqs. (16), (18), (19) will be referred to as the discrete auxiliary problem (AP). The inverse of $\boldsymbol{L}^{(h)}$ with boundary conditions (16), (18) is called the discrete Green's operator $\boldsymbol{G}^{(h)}$, so that the solution to the discrete AP is given by

$$u^{(h)} = \boldsymbol{G}^{(h)} g^{(h)}. \tag{20}$$

In this work, we are considering the Helmholtz equation (1) with $k^2 = \text{const}$. Therefore, we can solve the discrete AP (16), (18), (19) by separation of variables. Since the solution $u^{(h)}$ satisfies the boundary conditions (16), it can be represented using the 2D discrete inverse sine Fourier transform:

$$u_{s,t,p} = \frac{4}{S^2}\sum_{m=0}^{S}\sum_{n=0}^{S}\hat{u}_{s,m,n}\sin\frac{m\pi t}{S}\sin\frac{n\pi p}{S}, \tag{21a}$$

where

$$\hat{u}_{s,m,n} = \sum_{t=0}^{S}\sum_{p=0}^{S}u_{s,t,p}\sin\frac{m\pi t}{S}\sin\frac{n\pi p}{S}. \tag{21b}$$

As the right-hand side $g^{(h)}$ is defined on the grid $\mathbb{M}$ of (13), it can be artificially complemented with zeros on $\mathbb{N}\backslash\mathbb{M}$, and then representation (21) will apply to $g^{(h)}$ as well. Substituting representation (21a) for both $u^{(h)}$ and $g^{(h)}$ into Eqs. (19), (15), applying (21b), and using orthogonality of the grid functions $\sin\frac{m\pi t}{S}\sin\frac{n\pi p}{S}$, we obtain a system of disjoint one-dimensional finite difference equations in the x direction for $m = 1,\dots,S-1$ and $n = 1,\dots,S-1$:

$$\begin{aligned}\left(D_{xx}+\lambda_m^2+\lambda_n^2\right)\left(1+\frac{k^2h^2}{30}\right)\hat{u}_{\cdot,m,n} + \frac{h^4}{30}\lambda_m^2\lambda_n^2 D_{xx}\hat{u}_{\cdot,m,n} + \left(1-\frac{k^2h^2}{20}\right)k^2\hat{u}_{\cdot,m,n}\\ + \frac{h^2}{6}\left((\lambda_m^2+\lambda_n^2)D_{xx}+\lambda_m^2\lambda_n^2\right)\left(1+\frac{k^2h^2}{15}\right)\hat{u}_{\cdot,m,n} = \hat{g}_{\cdot,m,n},\end{aligned} \tag{22}$$

where $\lambda_m^2 = -\frac{4}{h^2}\sin^2\frac{m\pi}{2S}$. Each tridiagonal system (22) is solved using Thomas algorithm. Once all $\hat{u}_{s,m,n}$ have been determined from (22), the solution $u^{(h)}$ is reconstructed with the help of (21a). The overall complexity of this solution algorithm for the AP (16), (18), (19) is $\mathcal{O}(S^3\ln S)$.

3.2. Difference potentials

We recall that the individual scatterers are denoted by Ω_q, $q = 1,\dots,N$, with their boundaries $\Gamma_q = \partial\Omega_q$, and the common artificial outer boundary is denoted by Ω_0 with the boundary $\Gamma_0 = \partial\Omega_0$. Let us also denote the overall boundary by $\Gamma = \bigcup_{q=0}^{N}\Gamma_q$.

3.2.1. Grid boundary γ

Let $m \in \mathbb{M}$ be a node of the grid $\mathbb{M}$ of (13), and let $\mathbb{N}_m$ be the $3\times3\times3$ stencil of the operator $L^{(h)}$ of (15) centered at m. The domain $\Omega = \Omega_0 \setminus S_N$ splits $\mathbb{M}$ into two disjoint subsets of nodes: $\mathbb{M}^+ = \mathbb{M}\cap\Omega$ and $M^- = \mathbb{M}\backslash\mathbb{M}^+$. Then, on the grid $\mathbb{N}$ of (12) one can define another two subsets:

$$\mathbb{N}^+ = \bigcup_{m\in\mathbb{M}^+}\mathbb{N}_m \quad\text{and}\quad \mathbb{N}^- = \bigcup_{m\in\mathbb{M}^-}\mathbb{N}_m. \tag{23}$$

The intersection of $\mathbb{N}^+$ and $\mathbb{N}^-$ is a fringe of grid nodes that straddles the continuous boundary Γ (see Fig. 4):

$$\gamma = \mathbb{N}^+\cap\mathbb{N}^-. \tag{24}$$

One can define γ in a slightly different yet equivalent way. For $q = 0,1,\dots,N$, consider $\mathbb{M}_q^+ = \mathbb{M}\cap\Omega_q$ and $\mathbb{M}^- = \mathbb{M}\backslash\mathbb{M}_q^+$. Accordingly,

$$\mathbb{N}_q^+ = \bigcup_{m\in\mathbb{M}_q^+}\mathbb{N}_m,\quad \mathbb{N}_q^- = \bigcup_{m\in\mathbb{M}_q^-}\mathbb{N}_m,\quad\text{and}\quad \gamma_q = \mathbb{N}_q^+\cap\mathbb{N}_q^-. \tag{25}$$

The overall grid boundary γ of (24) is $\gamma = \bigcup_{q=0}^{N}\gamma_q$. It plays a fundamental role in the construction of our algorithm as the main equation to solve will be formulated with respect to an unknown grid function on γ, see Theorem 1 and Eq. (28). Once determined, this grid function on γ yields the density of a difference potential that reconstructs the solution on the entire grid set $\mathbb{N}^+$.

3.2.2. Discrete boundary equation with projection (BEP)

Let ξ_γ be a grid function defined on γ of (24). One extends it by zeros to the entire grid $\mathbb{N}$:

$$w^{(h)}\Big|_{(s,t,p)} = \begin{cases}\xi_\gamma, & (s,t,p)\in\gamma,\\ 0, & (s,t,p)\in\mathbb{N}\setminus\gamma.\end{cases}$$

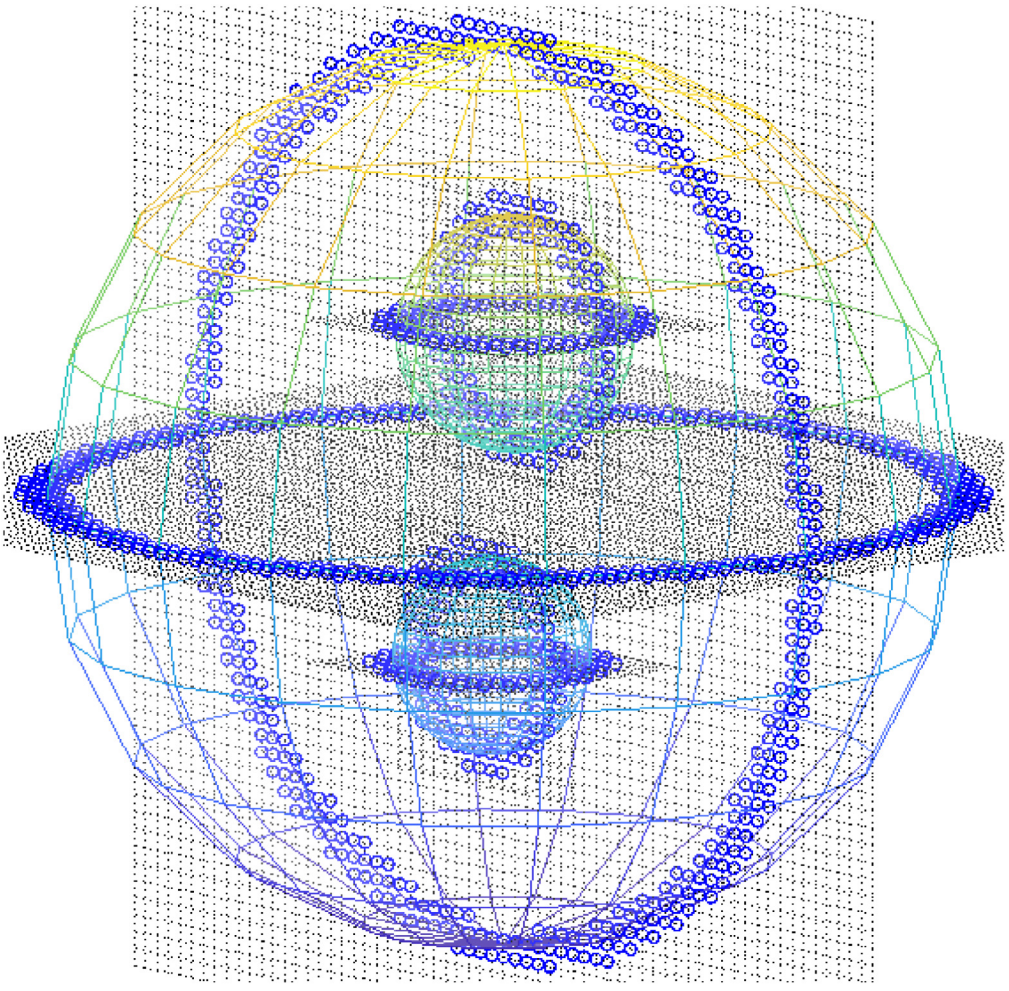

Fig. 4. Cross-sections of the grid boundary γ defined by (24).

The discrete trace operator is the restriction of a function $v^{(h)}$ defined on $\mathbb{N}$ to the grid boundary γ, i.e. $\boldsymbol{Tr}_{\gamma}^{(h)} v^{(h)} = v^{(h)}\Big|_{\gamma}$. Clearly, $\boldsymbol{Tr}_{\gamma}^{(h)} w^{(h)} = \xi_{\gamma}$. The difference potential with density ξ_{γ} is defined on the grid $\mathbb{N}^{+}$ of (23):

$$\boldsymbol{P}_{\mathbb{N}^{+}} \xi_{\gamma} \stackrel{\text{def}}{=} \boldsymbol{G}^{(h)}\Big(\boldsymbol{L}^{(h)} w^{(h)}\Big|_{\mathbb{M}^{-}}\Big), \tag{26}$$

where $\boldsymbol{G}^{(h)}$ is the discrete Green's operator (20). In other words, the potential $\boldsymbol{P}_{\mathbb{N}^{+}} \xi_{\gamma}$ of (26) is the solution on $\mathbb{N}^{+}$ of the discrete AP (16), (18), (19) driven by the source term:

$$g^{(h)}\Big|_{(s,t,p)} = \begin{cases} \boldsymbol{L}^{(h)} w^{(h)}\Big|_{(s,t,p)}, & (s,t,p) \in \mathbb{M}^{-}, \\ 0, & (s,t,p) \in \mathbb{M}^{+}. \end{cases}$$

The potential $\boldsymbol{P}_{\mathbb{N}^{+}} \xi_{\gamma}$ solves the homogeneous difference equation (14) on $\mathbb{M}^{+}$: $\boldsymbol{L}^{(h)} \boldsymbol{P}_{\mathbb{N}^{+}} \xi_{\gamma} = 0\big|_{\mathbb{M}^{+}}$.

The discrete boundary projection is the trace $\boldsymbol{Tr}_{\gamma}^{(h)}$ of the difference potential (26):

$$\boldsymbol{P}_{\gamma} \xi_{\gamma} \stackrel{\text{def}}{=} \boldsymbol{Tr}_{\gamma}^{(h)} \boldsymbol{P}_{\mathbb{N}^{+}} \xi_{\gamma} = \boldsymbol{Tr}_{\gamma}^{(h)} \boldsymbol{G}^{(h)}\Big(\boldsymbol{L}^{(h)} \xi_{\gamma}\Big|_{\mathbb{M}^{-}}\Big). \tag{27}$$

Theorem 1. *A grid function $u^{(h)}$ defined on $\mathbb{N}^{+}$ is a solution to the discrete homogeneous equation (14) on $\mathbb{M}^{+}$ if and only if its trace $\boldsymbol{Tr}_{\gamma}^{(h)} u^{(h)} = \xi_{\gamma}$ satisfies the discrete boundary equation with projection (BEP) on γ:*

$$\boldsymbol{P}_{\gamma} \xi_{\gamma} = \xi_{\gamma}. \tag{28}$$

The proof of Theorem 1 can be found in [11]. The BEP (28) is the key equation to be solved. If it holds, then the solution $u^{(h)}$ of (14) is reconstructed in the form of the difference potential (26).

The difference potential (26) approximates the continuous solution $u^{(scat)}$ to the scattering problem (1)–(4) provided that the discrete density ξ_γ is related to the boundary data of $u^{(scat)}$ on Γ (Dirichlet and Neumann) via the extension operator introduced in Section 3.2.3.

3.2.3. Extension operator

Hereafter, we assume that the grid is sufficiently fine so that $\gamma_{q_1} \cap \gamma_{q_2} = \emptyset$ if $q_1 \neq q_2$, see (25). Since in this work all domains Ω_q, $q = 0, \ldots, N$, are spherical, we can associate local spherical coordinates (r, θ, φ) with each of them so that the origin $r = 0$ is at the center of a given Ω_q. Denote the spherical Helmholtz operator in these coordinates by $\boldsymbol{L}_q$:

$$\boldsymbol{L}_q u = \frac{\partial^2 u}{\partial r^2} + \frac{2}{r}\frac{\partial u}{\partial r} + \frac{\Delta_{\theta,\varphi} u}{r^2} + k^2 u, \tag{29}$$

where $\Delta_{\theta,\varphi}$ is defined by (9). Equation-based differentiation of a given function u is differentiation under the assumption that u satisfies the Helmholtz equation (1) or, equivalently, equation $\boldsymbol{L}_q u = 0$.

Let $\boldsymbol{A}_q u \overset{\text{def}}{=} \boldsymbol{L}_q u - u_{rr}$, where $\boldsymbol{L}_q$ is given by (29). As $\boldsymbol{L}_q u = 0$, for the second derivative w.r.t. r we can write: $u_{rr} = -\boldsymbol{A}_q u \equiv -\frac{2}{r}\frac{\partial u}{\partial r} - \frac{\Delta_{\theta,\varphi} u}{r^2} - k^2 u$. Higher order derivatives w.r.t. r can be obtained by differentiating $\boldsymbol{A}_q u$:

$$\frac{\partial^j u}{\partial r^j} = -\frac{\partial^{j-2}\left\{\boldsymbol{A}_q u\right\}}{\partial r^{j-2}}. \tag{30}$$

From (30), it is clear that the second radial derivative $\frac{\partial^2 u}{\partial r^2}$ depends only on u and $\frac{\partial u}{\partial r}$ (and tangential derivatives via the Beltrami operator $\Delta_{\theta,\varphi}$). The third derivative $\frac{\partial^3 u}{\partial r^3}$, which corresponds to $j = 3$ in formula (30), depends on u, $\frac{\partial u}{\partial r}$, and $\frac{\partial^2 u}{\partial r^2}$, but substituting $\frac{\partial^2 u}{\partial r^2}$ from the previous case $j = 2$, we see that $\frac{\partial^3 u}{\partial r^3}$ also depends only on u and $\frac{\partial u}{\partial r}$. By continuing the differentiation and recursive substitution, we realize that all $\frac{\partial^n u}{\partial r^n}$ depend only on u and $\frac{\partial u}{\partial r}$ as well.

Let the grid point $d \in \gamma_q$, see (25), have coordinates (r, θ, φ) in the spherical system associated with Ω_q. The point $d_0 = (r_q, \theta, \varphi) \in \Gamma_q$ is the closest point to d on the sphere Γ_q of radius r_q. In general, $d_0 \notin \mathbb{N}$. Let $\rho = r - r_q$ be the distance (with sign) between d and d_0. Let $\boldsymbol{\xi}_{\Gamma_q} = \left(u, \frac{\partial u}{\partial r}\right)\Big|_{\Gamma_q}$ represent the Dirichlet and Neumann boundary data of u on the surface Γ_q. The equation-based extension operator from the continuous boundary Γ_q to the discrete boundary γ_q is defined point-wise. For every $d \in \gamma_q$, it is given by the Taylor's formula of order J centered at $d_0 \in \Gamma_q$:

$$\boldsymbol{Ex}_q\, \boldsymbol{\xi}_{\Gamma_q}\Big|_d \overset{\text{def}}{=} u + \frac{\partial u}{\partial r}\rho - \sum_{j=2}^{J} \frac{\rho^j}{j!} \frac{\partial^{j-2}\left\{\boldsymbol{A}_q u\right\}}{\partial r^{j-2}}\Bigg|_{d_0}. \tag{31}$$

For the entire γ_q, we will write:

$$\xi_{\gamma_q} = \boldsymbol{Ex}_q\, \boldsymbol{\xi}_{\Gamma_q}, \tag{32}$$

assuming that for each individual node $d \in \gamma_q$ the extension is obtained with the help of (31). As formula (31) is $\mathcal{O}(\rho^{J+1})$ accurate, then ξ_{γ_q} of (32) will converge to $u\big|_{\gamma_q}$ with the rate $\mathcal{O}(h^{J+1})$.

Moreover, the right-hand side of (31) depends only on u, $\frac{\partial u}{\partial r}$, and their tangential derivatives at the point d_0 (see the discussion after equation (30)). Consequently, the same is true regarding the right-hand side of (32). Therefore, we can consider a general sufficiently smooth vector function $\boldsymbol{\xi}_{\Gamma_q} = (\xi_0^q, \xi_1^q)$ on Γ_q, not necessarily the trace of a solution u to Eq. (1), and formally apply the extension operator $\boldsymbol{Ex}_q$ to it. Indeed, the right-hand side of (32) will depend only on ξ_0^q, ξ_1^q, their derivatives with respect to θ and φ, as well as r_q and the individual distances ρ for all nodes in γ_q. In particular, to compute the projection $\boldsymbol{P}_\gamma$ given by (27) in the form of a matrix, we will need to be able to apply the extension operator (31), (32) to spherical harmonics: $\xi_0(\theta, \varphi) = Y_\ell^{\mathrm{m}}(\theta, \varphi)$ and $\xi_1(\theta, \varphi) = Y_{\ell'}^{\mathrm{m}'}(\theta, \varphi)$, see Section 3.2.4. Since Y_ℓ^{m} are eigenfunctions of the Beltrami operator, $\Delta_{\theta,\varphi} Y_\ell^{\mathrm{m}} = -\ell(\ell+1) Y_\ell^{\mathrm{m}}$, for $(\xi_0^q, \xi_1^q) = (Y_\ell^{\mathrm{m}}, Y_{\ell'}^{\mathrm{m}'})$ formula (32) can be recast as

$$\xi_{\gamma_q} = A\xi_0^q + B\xi_1^q,$$

where

$$\begin{aligned} A =& 1 - \frac{\rho^6 \ell^3 (\ell+1)^3}{720 r^6} + (\ell(\ell+1))^2 \frac{\rho^4}{120}\left(\frac{\rho^2 k^2}{2r^4} - \frac{59\rho^2 - 36\rho r + 15 r^2}{3r^6}\right) \\ &+ \frac{\rho^2 \ell(\ell+1)}{120}\left(\frac{\rho^4 k^4}{2r^2} - \frac{\rho^2 k^2 \left(21\rho^2 - 16\rho r + 10 r^2\right)}{r^4} + \frac{100\rho^4 - 96\rho^3 r + 90\rho^2 r^2 - 80\rho r^3 + 60 r^4}{r^6}\right) \\ &- \frac{\rho^2 k^2}{720}\left(\rho^4 k^4 - \frac{6\rho^2 k^2 \left(4\rho^2 - 4\rho r + 5 r^2\right)}{r^2} + \frac{240\rho(\rho - r)\left(\rho^2 + r^2\right)}{r^4} + 360\right) \end{aligned}$$

and

$$B = \frac{(r-\rho)\,\rho^5 k^4}{120r} - \frac{(r-\rho)\left(\rho^2+r^2\right)\rho^3 k^2}{6r^3} + \frac{(\ell'(\ell'+1))^2\,(r-3\rho)\,\rho^5}{120r^5} + \frac{-r\rho^6 + r^2\rho^5 - r^3\rho^4 + r^4\rho^3 - r^5\rho^2 + r^6\rho}{r^6} + \ell'(\ell'+1)\frac{\rho^3}{60r^3}\left(\frac{37\rho^3 - 29\rho^2 r + 20\rho r^2 - 10r^3}{r^2} + \rho^2 k^2 (r-2\rho)\right).$$

Given that $\Gamma = \bigcup_{q=0}^{N} \Gamma_q$, we introduce

$$\boldsymbol{\xi}_\Gamma = \left(\boldsymbol{\xi}_{\Gamma_0}, \boldsymbol{\xi}_{\Gamma_1}, \ldots, \boldsymbol{\xi}_{\Gamma_N}\right)$$

and obtain the overall extension operator from Γ to $\gamma = \bigcup_{q=0}^{N} \gamma_q$ as juxtaposition of individual $\boldsymbol{Ex}_q$:

$$\xi_\gamma = \boldsymbol{Ex}\boldsymbol{\xi}_\Gamma = \left(\xi_{\gamma_0}, \xi_{\gamma_1}, \ldots, \xi_{\gamma_N}\right) = \left(\boldsymbol{Ex}_0\boldsymbol{\xi}_{\Gamma_0}, \boldsymbol{Ex}_1\boldsymbol{\xi}_{\Gamma_1}, \ldots, \boldsymbol{Ex}_N\boldsymbol{\xi}_{\Gamma_N}\right). \tag{33}$$

The choice of J in formula (31) is of central importance for the approximation of the continuous solution by the difference potential (26). As proved by Reznik [30,31] (see also [11, Part III, Section 1.4]), if $\boldsymbol{\xi}_\Gamma = \left(u^{(scat)}, \frac{\partial u^{(scat)}}{\partial r}\right)\Big|_\Gamma$ and $\xi_\gamma = \boldsymbol{Ex}\boldsymbol{\xi}_\Gamma$, see (33), then choosing J equal to the sum of the order of accuracy of the scheme plus the order of the differential equation that is being approximated, guarantees that the difference potential $\boldsymbol{P}_{\mathbb{N}^+\gamma}$ will converge to $u^{(scat)}\big|_{\mathbb{N}^+}$ with the design rate of the scheme. For the sixth order accurate scheme (14), (15), and the Helmholtz equation (1) that is second order, one should therefore choose $J = 8$ for sixth order convergence. It has, however, been repeatedly observed [23,32–34] that in practice a lower value of J is sufficient for guaranteeing the design rate of convergence. In the simulations of Section 4, we take $J = 6$ and still observe the $\mathcal{O}(h^6)$ convergence of the difference potential (26) to the continuous solution.

3.2.4. Boundary equations

Since the difference potential approximates the discrete solution to the Helmholtz equation on the grid as long as its density is obtained as extension of the boundary data of the continuous solution, we will be looking for $\boldsymbol{\xi}_\Gamma$ such that $\boldsymbol{Ex}\boldsymbol{\xi}_\Gamma$ satisfies the BEP (28), see Theorem 1.

Taking $\boldsymbol{\xi}_{\Gamma_q} = (\xi_0^q, \xi_1^q)$ as in Section 3.2.3, we expand each ξ_σ^q, $\sigma = 0, 1$, $q = 1, \ldots, N$, with respect to spherical harmonics:

$$\xi_\sigma^q(\theta,\varphi) = \sum_{\ell=0}^{L_q}\sum_{\mathrm{m}=-\ell}^{\ell} c_{\ell\mathrm{m}}^{(\sigma,q)} Y_\ell^{\mathrm{m}}(\theta,\varphi). \tag{34}$$

For a smooth ξ_σ^q on the sphere, its expansion with respect to spherical harmonics converges rapidly. Hence, truncation at even moderate values of L_q in formula (34) already guarantees sufficient accuracy. The specific values of L_q that we have used in our simulations are provided in Section 4. The coefficients $c_{\ell\mathrm{m}}^{(\sigma,q)}$ of expansion (34), $\sigma = 0, 1$, $q = 1, \ldots, N$, will eventually become the unknowns that we will be solving the BEP (28) for.

In the space of two-dimensional vector functions $\boldsymbol{\xi}_{\Gamma_q}$ on Γ_q, introduce a basis of spherical harmonics:

$$\begin{aligned} &\boldsymbol{\psi}_{\ell\mathrm{m}}^{(0,q)} = (Y_\ell^{\mathrm{m}}, 0), \quad \boldsymbol{\psi}_{\ell\mathrm{m}}^{(1,q)} = (0, Y_\ell^{\mathrm{m}}), \\ &\ell = 0, \ldots, L_q, \quad \mathrm{m} = -\ell, \ldots, 0, \ldots, \ell. \end{aligned} \tag{35}$$

Then, using (34) and (35), we can write:

$$\boldsymbol{\xi}_{\Gamma_q} = \sum_{\ell=0}^{L_q}\sum_{\mathrm{m}=-\ell}^{\ell} c_{\ell\mathrm{m}}^{(0,q)}\boldsymbol{\psi}_{\ell\mathrm{m}}^{(0,q)} + \sum_{\ell=0}^{L_q}\sum_{\mathrm{m}=-\ell}^{\ell} c_{\ell\mathrm{m}}^{(1,q)}\boldsymbol{\psi}_{\ell\mathrm{m}}^{(1,q)}. \tag{36}$$

Applying the extension operator (31), (32) to $\boldsymbol{\xi}_{\Gamma_q}$ in the form (36), we have:

$$\xi_{\gamma_q} = \boldsymbol{Ex}_q\boldsymbol{\xi}_{\Gamma_q} = \sum_{\ell=0}^{L_q}\sum_{\mathrm{m}=-\ell}^{\ell} c_{\ell\mathrm{m}}^{(0,q)}\boldsymbol{Ex}_q\boldsymbol{\psi}_{\ell\mathrm{m}}^{(0,q)} + \sum_{\ell=0}^{L_q}\sum_{\mathrm{m}=-\ell}^{\ell} c_{\ell\mathrm{m}}^{(1,q)}\boldsymbol{Ex}_q\boldsymbol{\psi}_{\ell\mathrm{m}}^{(1,q)}, \tag{37}$$

and according to (33),

$$\xi_\gamma = \left(\xi_{\gamma_0}, \xi_{\gamma_1}, \ldots, \xi_{\gamma_N}\right), \tag{38}$$

where ξ_{γ_q}, $q = 0, \ldots, N$, are given by (37).

For future convenience, let us introduce the grid functions $\tilde{\xi}_{\gamma_q}$, $q = 0, \ldots, N$, each defined on the entire grid boundary $\gamma = \bigcup_{q=0}^{N} \gamma_q$, such that

$$\tilde{\xi}_{\gamma_q} = \begin{cases} \xi_{\gamma_q}, & \text{on } \gamma_q, \\ 0, & \text{on } \gamma \backslash \gamma_q. \end{cases} \tag{39}$$

Then, instead of (38) we can write:

$$\xi_\gamma = \sum_q \tilde{\xi}_{\gamma_q}. \tag{40}$$

Substituting (40) into the BEP (28) and taking into account (37), we obtain a system of linear algebraic equations with respect to the coefficients $c_{\ell \mathrm{m}}^{(0,q)}$ and $c_{\ell \mathrm{m}}^{(1,q)}$ of the expansion (36). Indeed, first we write:

$$\sum_q \underbrace{(\boldsymbol{P}_\gamma - \boldsymbol{I}_\gamma)}_{\stackrel{\text{def}}{=} \boldsymbol{Q}_\gamma} \tilde{\xi}_{\gamma_q} = 0. \tag{41}$$

Then, using representation (37), from (41) we have:

$$\sum_q \left(\sum_{\ell=0}^{L_q} \sum_{\mathrm{m}=-\ell}^{\ell} c_{\ell \mathrm{m}}^{(0,q)} \boldsymbol{Q}_\gamma \widetilde{\boldsymbol{E}\boldsymbol{x}}_q \boldsymbol{\psi}_{\ell \mathrm{m}}^{(0,q)} + \sum_{\ell=0}^{L_q} \sum_{\mathrm{m}=-\ell}^{\ell} c_{\ell \mathrm{m}}^{(1,q)} \boldsymbol{Q}_\gamma \widetilde{\boldsymbol{E}\boldsymbol{x}}_q \boldsymbol{\psi}_{\ell \mathrm{m}}^{(1,q)} \right) = 0, \tag{42}$$

where similarly to (39), the operator $\widetilde{\boldsymbol{E}\boldsymbol{x}}_q$ yields a grid function on the entire γ:

$$\widetilde{\boldsymbol{E}\boldsymbol{x}}_q \boldsymbol{\psi}_{\ell \mathrm{m}}^{(\sigma,q)} = \begin{cases} \boldsymbol{E}\boldsymbol{x}_q \boldsymbol{\psi}_{\ell \mathrm{m}}^{(\sigma,q)}, & \text{on } \gamma_q, \\ 0, & \text{on } \gamma \backslash \gamma_q, \end{cases} \qquad \sigma = 0, 1. \tag{43}$$

Each $\boldsymbol{Q}_\gamma \widetilde{\boldsymbol{E}\boldsymbol{x}}_q \boldsymbol{\psi}_{\ell \mathrm{m}}^{(0,q)}$ and $\boldsymbol{Q}_\gamma \widetilde{\boldsymbol{E}\boldsymbol{x}}_q \boldsymbol{\psi}_{\ell \mathrm{m}}^{(1,q)}$ in Eq. (42) is a grid function on γ. It is obtained by applying the projection $\boldsymbol{Q}_\gamma \equiv \boldsymbol{P}_\gamma - \boldsymbol{I}_\gamma$ to the corresponding density (43). The application of $\boldsymbol{Q}_\gamma$ requires solving the AP, see Section 3.1. For the chosen basis (35), all $\boldsymbol{Q}_\gamma \widetilde{\boldsymbol{E}\boldsymbol{x}}_q \boldsymbol{\psi}_{\ell \mathrm{m}}^{(0,q)}$ and $\boldsymbol{Q}_\gamma \widetilde{\boldsymbol{E}\boldsymbol{x}}_q \boldsymbol{\psi}_{\ell \mathrm{m}}^{(1,q)}$ can be pre-computed and subsequently considered known. Then, Eq. (42) becomes a linear system for $c_{\ell \mathrm{m}}^{(0,q)}$ and $c_{\ell \mathrm{m}}^{(1,q)}$. It has $L \equiv 2 \sum_q (1 + L_q)^2$ unknowns and as many equations as the number of nodes in the overall grid boundary γ, see (24) or (25); we will denote this number $|\gamma|$.

As the BEP (28) is equivalent to the Helmholtz equation (1) discretized using the scheme (14), (15) on the grid $\mathbb{N}^+$ of (23) (see Theorem 1), the resulting system (42) provides a discrete approximation the Helmholtz equation (1) reduced to the continuous boundary Γ.

Note that, the pre-computation of the vectors $\boldsymbol{Q}_\gamma \widetilde{\boldsymbol{E}\boldsymbol{x}}_q \boldsymbol{\psi}_{\ell \mathrm{m}}^{(0,q)}$ and $\boldsymbol{Q}_\gamma \widetilde{\boldsymbol{E}\boldsymbol{x}}_q \boldsymbol{\psi}_{\ell \mathrm{m}}^{(1,q)}$ is the most computationally intensive part of the entire algorithm. Its actual runtime cost is still affordable though because each of these vectors requires solving the same AP (Section 3.1) where only the right-hand side changes. Moreover, as the right-hand sides are independent, the solution is easily parallelizable. Another important consideration is that the vectors $\boldsymbol{Q}_\gamma \widetilde{\boldsymbol{E}\boldsymbol{x}}_q \boldsymbol{\psi}_{\ell \mathrm{m}}^{(0,q)}$ and $\boldsymbol{Q}_\gamma \widetilde{\boldsymbol{E}\boldsymbol{x}}_q \boldsymbol{\psi}_{\ell \mathrm{m}}^{(1,q)}$ need to be computed only once ahead of time. After that, a broad range of scattering problems that involve various incident fields and various types of scattering on the surface (sound-soft, sound-hard, etc.) can be solved at a low individual cost per problem with no need to recompute $\boldsymbol{Q}_\gamma \widetilde{\boldsymbol{E}\boldsymbol{x}}_q \boldsymbol{\psi}_{\ell \mathrm{m}}^{(0,q)}$ and $\boldsymbol{Q}_\gamma \widetilde{\boldsymbol{E}\boldsymbol{x}}_q \boldsymbol{\psi}_{\ell \mathrm{m}}^{(1,q)}$ (see Section 3.2.6 for further detail).

3.2.5. Boundary conditions

System (42) needs to be supplemented by the boundary conditions on Γ, which consist of the physical boundary conditions on Γ_q, $q = 1, \ldots, N$, and the BGT radiation condition on Γ_0. A key advantage of the MDP is that since the unknowns in system (42) are coefficients of the expansion (36) at the boundary Γ, the boundary conditions never need to be approximated on the grid. Indeed, a boundary condition for the Helmholtz equation is a relation between the solution, its first normal derivative, and, maybe, some tangential derivatives, at the boundary. Any such relation can be easily recast as a relation between the coefficients $c_{\ell \mathrm{m}}^{(0,q)}$ and $c_{\ell \mathrm{m}}^{(1,q)}$ of expansion (36), which pertains only to the boundary and does not involve any approximation on the volumetric grid. As expansion (36) is finite, a representation of the boundary condition via the coefficients $c_{\ell \mathrm{m}}^{(0,q)}$ and $c_{\ell \mathrm{m}}^{(1,q)}$ will not be exact, but will have spectral accuracy independent of the grid size. A component of the algorithm that does depend on the grid though is system (42), which enforces the governing Helmholtz equation itself. This system has the same unknowns $c_{\ell \mathrm{m}}^{(0,q)}$ and $c_{\ell \mathrm{m}}^{(1,q)}$, but is derived from the discrete BEP (28) on the grid boundary γ.

The BGT radiation condition $B_6 u = 0$, see (10), is a relation between u, its tangential derivatives in $\Delta_{\theta,\varphi} u$, and $\frac{\partial u}{\partial r}$ at the artificial outer boundary Γ_0. Substituting ξ_0^0 for u and ξ_1^0 for $\frac{\partial u}{\partial r}$ in the form (34) under the operator B_6, taking into account that $\Delta_{\theta,\varphi} Y_\ell^{\mathrm{m}} = -\ell(\ell+1) Y_\ell^{\mathrm{m}}$, and using the orthogonality of the spherical harmonics Y_ℓ^{m}, we recast the boundary condition

$B_6 u = 0$ as a system of linear equations with respect to the coefficients $c_{\ell\mathrm{m}}^{(0,0)}$ and $c_{\ell\mathrm{m}}^{(1,0)}$, $\ell = 0, \ldots, L_0$, $\mathrm{m} = -\ell, \ldots, \ell$:

$$\begin{aligned}
&\left(\frac{18}{R_0^5} - \frac{6ik}{R_0^4}\right)(\ell(\ell+1))^2 c_{\ell\mathrm{m}}^{(1,0)} - \left(-\frac{32ik^3}{R_0^2} + \frac{288k^2}{R_0^3} + \frac{708ik}{R_0^4} - \frac{444}{R_0^5}\right)(\ell(\ell+1)) c_{\ell\mathrm{m}}^{(1,0)} \\
&+\left(-32ik^5 + \frac{480k^4}{R_0} + \frac{2400ik^3}{R_0^2} - \frac{4800k^2}{R_0^3} - \frac{3600ik}{R_0^4} + \frac{720}{R_0^5}\right) c_{\ell\mathrm{m}}^{(1,0)} \\
&+\frac{1}{R_0^6}(\ell(\ell+1))^3 c_{\ell\mathrm{m}}^{(0,0)} + \left(-\frac{18k^2}{R_0^4} - \frac{108ik}{R_0^5} + \frac{136}{R_0^6}\right)(\ell(\ell+1))^2 c_{\ell\mathrm{m}}^{(0,0)} \\
&-\left(-\frac{48k^4}{R_0^2} - \frac{544ik^3}{R_0^3} + \frac{1980k^2}{R_0^4} + \frac{2664ik}{R_0^5} - \frac{1044}{R_0^6}\right)(\ell(\ell+1)) c_{\ell\mathrm{m}}^{(0,0)} \\
&+\left(-32k^6 - \frac{512ik^5}{R_0} + \frac{2880k^4}{R_0^2} + \frac{7200ik^3}{R_0^3} - \frac{8400k^2}{R_0^4} - \frac{4320ik}{R_0^5} + \frac{720}{R_0^6}\right) c_{\ell\mathrm{m}}^{(0,0)} = 0,
\end{aligned} \tag{44}$$

where R_0 is the radius of the sphere Γ_0. The boundary conditions on Γ_q for $q = 1, \ldots, N$ become:

$$\xi_0^q = -u^{(inc)}, \quad \text{if } \Omega_q \text{ is a sound-soft body,} \tag{45a}$$

or

$$\xi_1^q = -\frac{\partial u^{(inc)}}{\partial n_q}, \quad \text{if } \Omega_q \text{ is a sound-hard body,} \tag{45b}$$

where $\frac{\partial}{\partial n_q}$ is the normal derivative on Γ_q. The Dirichlet boundary condition (45a) implies that the coefficients $c_{\ell\mathrm{m}}^{(0,q)}$ for $\ell = 0, \ldots, L_q$, $\mathrm{m} = -\ell, \ldots, \ell$ are known:

$$c_{\ell\mathrm{m}}^{(0,q)} = -\int_0^{2\pi}\int_0^{\pi} u^{(inc)}(\theta,\varphi) Y_\ell^{\mathrm{m}}(\theta,\varphi)\sin\theta\, d\theta\, d\varphi. \tag{46a}$$

Similarly, the Neumann boundary condition (45b) implies that the coefficients $c_{\ell\mathrm{m}}^{(1,q)}$ for $\ell = 0, \ldots, L_q$, $\mathrm{m} = -\ell, \ldots, \ell$ are known:

$$c_{\ell\mathrm{m}}^{(1,q)} = -\int_0^{2\pi}\int_0^{\pi} \frac{\partial u^{(inc)}}{\partial n_q}(\theta,\varphi) Y_\ell^{\mathrm{m}}(\theta,\varphi)\sin\theta\, d\theta\, d\varphi. \tag{46b}$$

In our simulations (see Section 4), for each scatterer Ω_q we use either Eqs. (46a) or Eqs. (46b). For the implementation of Robin boundary conditions, see [35,36]. In fact, any well-posed boundary condition for the second order differential equation (1) can be formulated as a relation between u and $\frac{\partial u}{\partial n}$ on Γ_q, $q = 1, \ldots, N$ (maybe, nonlocal). Hence, it can be reduced to linear algebraic equations with respect to $c_{\ell\mathrm{m}}^{(0,q)}$ and $c_{\ell\mathrm{m}}^{(1,q)}$.

Eqs. (44) and (46) supplement the main linear system (42). The combined system (42), (44), (46) is to be solved with respect to the remaining unknown coefficients $c_{\ell\mathrm{m}}^{(0,q)}$ and $c_{\ell\mathrm{m}}^{(1,q)}$. After that, the density ξ_γ of the difference potential (26) is reconstructed with the help of (37), (38) and the discrete solution on the grid $\mathbb{N}^+$ is obtained in the form $u^{(h)} = P_{\mathbb{N}^+\gamma}\xi_\gamma$.

3.2.6. Solution of the linear system

The dimension of system (42) is $|\gamma| \times L$, where $L = 2\sum_q (1+L_q)^2$. To put this system together, one needs to solve one discrete AP (16), (18), (19) per unknown (see Section 3.1), i.e., L discrete APs altogether.[2] There are $2(1+L_0)^2$ more equations in (44), yet these equations do not bring any extra unknowns. Moreover, it is easy to eliminate $c_{\ell\mathrm{m}}^{(1,0)}$ from (44), i.e., express it via $c_{\ell\mathrm{m}}^{(0,0)}$ for each pair of values (ℓ, m) (or the other way around), and then substitute into (42). Hence, Eqs. (44) do not need to be considered as additional equations for (42). Relations (46) do not need to be interpreted as additional linear equations either. These equations are trivial and it is easier to substitute the known coefficients (46a) or (46b) into (42). This will make Eqs. (42) inhomogeneous and further reduce the overall number of unknowns. Since one set of coefficients (46a) or (46b) is known per scatterer $q = 1, \ldots, N$, and one set of coefficients is expressed via the other for $q = 0$, the remaining number of unknowns in the system is $L' = \sum_{q=0}^{N}(1+L_q)^2 = L/2$.

The dimensions L_q in (35) are typically low. Consequently, for all sufficiently fine grids the resulting linear system of dimension $|\gamma| \times L'$ is overdetermined and needs to be solved in the sense of least squares (often, $|\gamma| \gg L'$). However, as long as the original scattering problem (1)–(4) has a unique solution, the value of the minimum obtained by least squares will be zero within the accuracy of the finite difference approximation, i.e., $\mathcal{O}(h^6)$.

Let us write the system to be solved by least squares as

$$\boldsymbol{A}\boldsymbol{c} = \boldsymbol{f},$$

[2] In fact, due to symmetries one can solve fewer discrete APs than the total number of basis functions in (35) for all q, see [37, Section 5.1] for detail.

where $\boldsymbol{A}$ is $|\gamma| \times L'$, $\boldsymbol{c}$ is an L'-dimensional vector of all unknown coefficients $c_{\ell m}^{(0,q)}$ and $c_{\ell m}^{(1,q)}$, and $\boldsymbol{f}$ is a $|\gamma|$-dimensional vector of the right-hand side formed using the known data (46). The matrix $\boldsymbol{A}$ consists of those columns $Q_\gamma \widetilde{E x}_q \psi_{\ell m}^{(0,q)}$ and $Q_\gamma \widetilde{E x}_q \psi_{\ell m}^{(1,q)}$, see (42), that correspond to the unknown coefficients $c_{\ell m}^{(0,q)}$ and $c_{\ell m}^{(1,q)}$. The vector $\boldsymbol{f}$ can be represented as $\boldsymbol{f} = B\tilde{\boldsymbol{c}}$, where $\tilde{\boldsymbol{c}}$ is the vector of known coefficients (46a), (46b) of dimension $\tilde{L} = \sum_{q=1}^{N}(1+L_q)^2$, and B is a fixed matrix of dimension $|\gamma| \times \tilde{L}$. The columns of the matrix B are those $Q_\gamma \widetilde{E x}_q \psi_{\ell m}^{(0,q)}$ and $Q_\gamma \widetilde{E x}_q \psi_{\ell m}^{(1,q)}$ that correspond to the known coefficients (46a) and (46b). Altogether, the system we are solving by least squares is

$$\boldsymbol{A}\boldsymbol{c} = B\tilde{\boldsymbol{c}}. \tag{47}$$

The least squares solution of (47) is computed by means of QR factorization:

$$\boldsymbol{A}_{|\gamma|\times L'} = \boldsymbol{Q}_{|\gamma|\times L'} \boldsymbol{R}_{L'\times L'}, \tag{48}$$

where $\boldsymbol{Q}$ is orthogonal and $\boldsymbol{R}$ is upper triangular. Substituting the factorized form of $\boldsymbol{A}$ into (47), we have:

$$\boldsymbol{c} = \boldsymbol{R}^{-1}\boldsymbol{Q}^* B\tilde{\boldsymbol{c}} \equiv D\tilde{\boldsymbol{c}}, \tag{49}$$

where the matrix D has low dimension: $L' \times \tilde{L}$. It is therefore advantageous to pre-compute it ahead of time. Then, changing $\tilde{\boldsymbol{c}}$ will entail only a very small additional cost for getting $\boldsymbol{c}$. It means that computing the scattering solution for a different incident field becomes very inexpensive. For example, one can change the incidence angles in (2) or move the center of the spherical wave in (3). Then, to obtain the new solution, one only needs to re-evaluate the integrals in (46), apply the matrix D in (49), obtain ξ_γ, see (37), (38), and compute the difference potential (26). Computing the difference potential requires solving the discrete AP (Section 3.1), which is done by separation of variables/FFT at log-linear cost.

In fact, even a broader class of similar problems (beyond those that only involve a different incident field) can be solved at a low additional cost per problem. For example, changing the type of scattering on a given Ω_q, say, from Dirichlet to Neumann, will swap the respective sets of coefficients $c_{\ell m}^{(0,q)}$ and $c_{\ell m}^{(1,q)}$, see (46), so that those that used to be known become unknown and the other way around. This will cause the corresponding changes in the composition of columns of the matrices $\boldsymbol{A}$ and B in (47). However, it will not require any additional solutions of the discrete AP (16), (18), (19), because all $Q_\gamma \widetilde{E x}_q \psi_{\ell m}^{(0,q)}$ and $Q_\gamma \widetilde{E x}_q \psi_{\ell m}^{(1,q)}$ in (42) remain the same. Consequently, the only additional cost will be that of another QR factorization (48). One can further reduce it with the help of the QR updating algorithms, see, e.g., [38].

4. Results

We consider the scattering of a plane wave (2) or spherical wave (3) about two obstacles. The first obstacle is a sound-hard sphere of radius 0.6 centered at (0.65, 0.65, 0.65). The second obstacle is a sound-soft sphere of radius 0.5 centered at (−0.65, −0.65, −0.65). The artificial outer boundary Γ_0 is a sphere of radius $R_0 = 2.3$ centered at the origin, see (5). The solution at Γ_0 it is terminated by the sixth order BGT radiation condition $B_6 u = 0$, see (10) and (44).

The auxiliary domain (11) is a cube $\widetilde{\Omega} = [-2.8, 2.8] \times [-2.8, 2.8] \times [-2.8, 2.8]$. The AP is discretized on a sequence of a uniform Cartesian grids $32 \times 32 \times 32$ through $512 \times 512 \times 512$.

Neither of the dimensions L_q, $q = 0, 1, 2$, see Eqs. (34), (35), exceeds the value of 31 in our simulations. This guarantees that the truncated part of the expansion (34) will not exceed 10^{-11} for any of our test solutions. The specific values of L_0, L_1, and L_2 are provided in Tables 1 through 9, where L_0 is the number of basis functions on the artificial outer boundary, L_1 is that on the sound-hard sphere in the first octant, and L_2 is that on the remaining sound-soft sphere.

To assess the grid convergence, we evaluate the maximum norm on the grid $\mathbb{N}^+$ of the difference between the numerical solutions obtained on consecutive grids:

$$\|u^{(h)} - u^{(2h)}\|_\infty.$$

In Fig. 5, we present the complex amplitude of the field scattered about the two spheres described in the beginning of this section. The incident plane wave is given by (2) with $\vartheta_{inc} = 45°$ and $\phi_{inc} = 55°$. In Fig. 5a, cross-sections of the field amplitude are shown along several Cartesian planes. Fig. 5b shows isosurfaces of the complex amplitude in 3D, as well as cross-sections through the origin projected onto the walls of the auxiliary cube.

In Tables 1 through 4, we show the error and convergence rate for the scattering of plane waves with incidence directions $(\vartheta_{inc}, \phi_{inc}) = (0°, 0°)$, $(5°, 5°)$, $(10°, 0°)$, and $(0°, 10°)$ and wavenumbers $k = 1$, 5, and 10. The tables clearly demonstrate the designed sixth order rate of grid convergence.

The error in numerical simulation of waves by finite differences (or finite elements) depends on the wavenumber k, see [39]. Specifically, for the computational domain of a fixed size, the error scales as $h^p k^{p+1}$, where h is the grid size and p is the order of accuracy. Consequently, to maintain a given accuracy, the number of points per wavelength $\propto (kh)^{-1}$ may not remain constant. It must increase proportionally to $k^{1/p}$, the effect known as pollution. For higher order schemes the pollution growth is slower than for lower order schemes.

To demonstrate the pollution effect, we need to have an analytic exact solution so that to be able to compute the actual error. We construct this solution by placing the pole x_0 of the spherical wave (3) at the center of one of the spheres: $x_0 = (0.65, 0.65, 0.65)$, and interpreting

$$u(\boldsymbol{x}) \equiv u^{(scat)}(\boldsymbol{x}) = \frac{e^{ik(\|\boldsymbol{x}-\boldsymbol{x}_0\|)}}{\|\boldsymbol{x}-\boldsymbol{x}_0\|}, \quad \boldsymbol{x} \in \Omega,$$

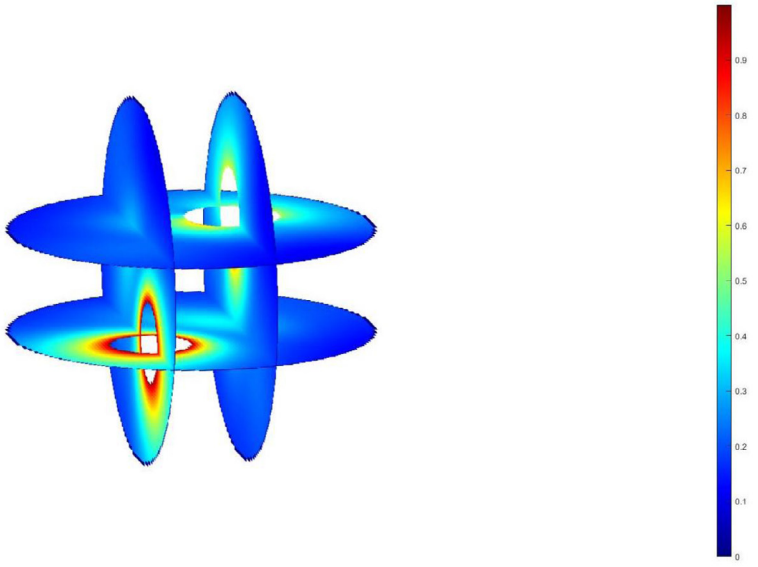

(a) Cross-sections of the magnitude of the scattered field.

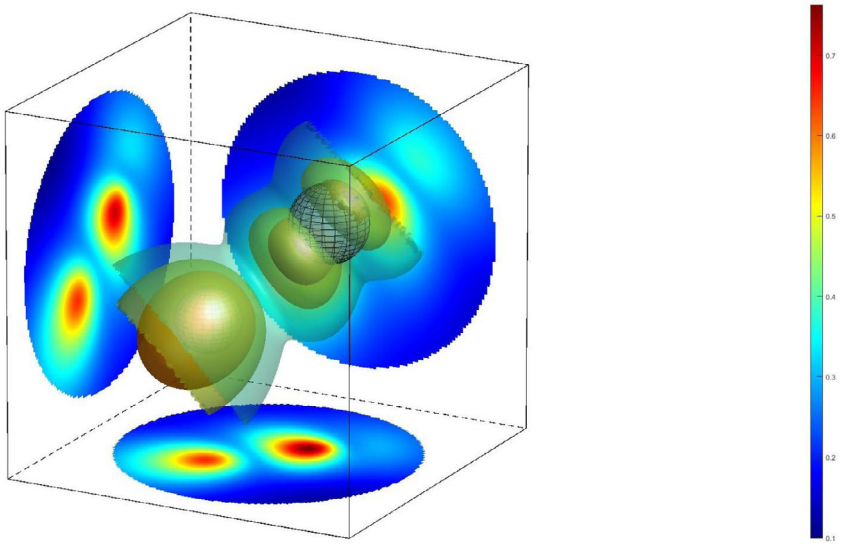

(b) Isosurfaces of the magnitude of the scattered field at 0.2652, 0.3815, and 0.5488 and cross-sections through the origin projected onto the walls of the auxiliary cube.

Fig. 5. Scattering of a plane wave about two spherical obstacles; $\vartheta_{inc} = 45°$, $\phi_{inc} = 55°$.

Table 1
Scattering of a plane wave (2) with $\vartheta_{inc} = 0°$, $\phi_{inc} = 0°$.

Grid	h	$k = 1$, $\{L_q\} = \{17, 11, 11\}$		$k = 5$, $\{L_q\} = \{31, 19, 18\}$		$k = 10$, $\{L_q\} = \{31, 24, 22\}$	
		$\|u^{(h)} - u^{(2h)}\|_\infty$	Rate	$\|u^{(h)} - u^{(2h)}\|_\infty$	Rate	$\|u^{(h)} - u^{(2h)}\|_\infty$	Rate
64	0.088	$1.1135 \cdot 10^{-2}$	–	$1.0430 \cdot 10^{2}$	–	2.2111	–
128	0.044	$1.0730 \cdot 10^{-4}$	6.69	$1.5327 \cdot 10^{-3}$	16.05	$7.0012 \cdot 10^{-3}$	8.30
256	0.022	$7.8706 \cdot 10^{-7}$	7.09	$1.0832 \cdot 10^{-5}$	7.14	$6.4567 \cdot 10^{-5}$	6.76
512	0.011	$6.7534 \cdot 10^{-9}$	6.86	$7.0310 \cdot 10^{-8}$	7.26	$4.9136 \cdot 10^{-7}$	7.03

as the scattered field to solve for outside the two scatterers, i.e., on $\Omega = \Omega_0 \backslash S_N$. The boundary data on Γ_1 and Γ_2 are taken directly from the solution $u^{(scat)}(x)$.

Table 2
Scattering of a plane wave (2) with $\vartheta_{inc} = 5°$, $\phi_{inc} = 5°$.

Grid	h	$k = 1$, $\{L_q\} = \{16, 11, 11\}$		$k = 5$, $\{L_q\} = \{31, 19, 17\}$		$k = 10$, $\{L_q\} = \{31, 24, 22\}$	
		$\|u^{(h)} - u^{(2h)}\|_\infty$	Rate	$\|u^{(h)} - u^{(2h)}\|_\infty$	Rate	$\|u^{(h)} - u^{(2h)}\|_\infty$	Rate
64	0.088	$1.0808 \cdot 10^{-2}$	–	$1.0735 \cdot 10^{2}$	–	2.2013	–
128	0.044	$1.0887 \cdot 10^{-4}$	6.63	$1.7101 \cdot 10^{-3}$	15.93	$6.8420 \cdot 10^{-3}$	8.32
256	0.022	$8.0673 \cdot 10^{-7}$	7.07	$9.6635 \cdot 10^{-6}$	7.46	$5.7465 \cdot 10^{-5}$	6.89
512	0.011	$7.5688 \cdot 10^{-9}$	6.73	$6.3080 \cdot 10^{-8}$	7.25	$4.4879 \cdot 10^{-7}$	7.00

Table 3
Scattering of a plane wave (2) with $\vartheta_{inc} = 0°$, $\phi_{inc} = 10°$.

Grid	h	$k = 1$, $\{L_q\} = \{17, 11, 11\}$		$k = 5$, $\{L_q\} = \{31, 19, 18\}$		$k = 10$, $\{L_q\} = \{31, 24, 22\}$	
		$\|u^{(h)} - u^{(2h)}\|_\infty$	Rate	$\|u^{(h)} - u^{(2h)}\|_\infty$	Rate	$\|u^{(h)} - u^{(2h)}\|_\infty$	Rate
64	0.088	$1.1135 \cdot 10^{-2}$	–	$1.0430 \cdot 10^{2}$	–	2.2111	–
128	0.044	$1.0730 \cdot 10^{-4}$	6.69	$1.5327 \cdot 10^{-3}$	16.05	$7.0012 \cdot 10^{-3}$	8.30
256	0.022	$7.8706 \cdot 10^{-7}$	7.09	$1.0832 \cdot 10^{-5}$	7.14	$6.4568 \cdot 10^{-5}$	6.76
512	0.011	$6.7534 \cdot 10^{-9}$	6.86	$7.0310 \cdot 10^{-8}$	7.26	$4.9137 \cdot 10^{-7}$	7.03

Table 4
Scattering of a plane wave (2) with $\vartheta_{inc} = 10°$, $\phi_{inc} = 0°$.

Grid	h	$k = 1$, $\{L_q\} = \{16, 11, 11\}$		$k = 5$, $\{L_q\} = \{31, 19, 17\}$		$k = 10$, $\{L_q\} = \{31, 24, 22\}$	
		$\|u^{(h)} - u^{(2h)}\|_\infty$	Rate	$\|u^{(h)} - u^{(2h)}\|_\infty$	Rate	$\|u^{(h)} - u^{(2h)}\|_\infty$	Rate
64	0.088	$1.0490 \cdot 10^{-2}$	–	$1.1088 \cdot 10^{2}$	–	2.3013	–
128	0.044	$1.1093 \cdot 10^{-4}$	6.56	$1.9018 \cdot 10^{-3}$	15.83	$7.4014 \cdot 10^{-3}$	8.28
256	0.022	$8.1217 \cdot 10^{-7}$	7.09	$9.4656 \cdot 10^{-6}$	7.65	$5.7444 \cdot 10^{-5}$	7.00
512	0.011	$7.5751 \cdot 10^{-9}$	6.74	$6.3881 \cdot 10^{-8}$	7.21	$4.2852 \cdot 10^{-7}$	7.06

Table 5
Pollution effect for the sixth order accurate MDP; $\{L_q\} = \{31, 1, 28\}$.

Grid	h	k	Error
$128 \times 128 \times 128$	0.044	4.41636	$6.17076 \cdot 10^{-6}$
$256 \times 256 \times 256$	0.022	8	$1.22301 \cdot 10^{-6}$
$512 \times 512 \times 512$	0.011	14.4916	$1.97805 \cdot 10^{-6}$

Table 6
Scattering of a spherical wave (3) with $x_0 = (5, 5, 5)$.

Grid	h	$k = 1$, $\{L_q\} = \{19, 11, 10\}$		$k = 5$, $\{L_q\} = \{31, 17, 15\}$		$k = 10$, $\{L_q\} = \{31, 23, 21\}$	
		$\|u^{(h)} - u^{(2h)}\|_\infty$	Rate	$\|u^{(h)} - u^{(2h)}\|_\infty$	Rate	$\|u^{(h)} - u^{(2h)}\|_\infty$	Rate
64	0.088	$6.5459 \cdot 10^{-4}$	–	$7.4918 \cdot 10^{-3}$	–	$2.7413 \cdot 10^{-1}$	–
128	0.044	$9.4720 \cdot 10^{-6}$	6.11	$1.2215 \cdot 10^{-4}$	5.93	$5.1117 \cdot 10^{-4}$	9.06
256	0.022	$1.0529 \cdot 10^{-7}$	6.49	$9.4567 \cdot 10^{-7}$	7.01	$6.0062 \cdot 10^{-6}$	6.41
512	0.011	$9.0059 \cdot 10^{-10}$	6.86	$6.4622 \cdot 10^{-9}$	7.19	$6.2670 \cdot 10^{-8}$	6.58

Table 7
Scattering of a spherical wave (3) with $x_0 = (-5, 5, 5)$.

Grid	h	$k = 1$, $\{L_q\} = \{19, 11, 10\}$		$k = 5$, $\{L_q\} = \{31, 17, 15\}$		$k = 10$, $\{L_q\} = \{31, 23, 21\}$	
		$\|u^{(h)} - u^{(2h)}\|_\infty$	Rate	$\|u^{(h)} - u^{(2h)}\|_\infty$	Rate	$\|u^{(h)} - u^{(2h)}\|_\infty$	Rate
64	0.088	$9.7449 \cdot 10^{-4}$	–	$2.2162 \cdot 10^{-2}$	–	$2.4335 \cdot 10^{-1}$	–
128	0.044	$1.7645 \cdot 10^{-5}$	5.78	$1.5893 \cdot 10^{-4}$	7.12	$1.0561 \cdot 10^{-3}$	7.84
256	0.022	$8.6684 \cdot 10^{-8}$	7.66	$1.4670 \cdot 10^{-6}$	6.75	$8.1243 \cdot 10^{-6}$	7.02
512	0.011	$9.7760 \cdot 10^{-10}$	6.47	$9.2023 \cdot 10^{-9}$	7.31	$6.6165 \cdot 10^{-8}$	6.94

Table 5 illustrates the pollution effect. The order of accuracy of the core scheme (14), (15) is $p = 6$. We choose the value of $k = 8$ for the grid of dimension $256 \times 256 \times 256$, and then vary h and change k synchronously as $k \propto h^{-6/7}$. From Table 5, we see that the error remains roughly the same as long as $h^6 k^7 = \text{const}$.

In Tables 6 through 9, we demonstrate the sixth order of grid convergence for the scattering of spherical waves (3) that originate at $x_0 = (5, 5, 5)$, $(-5, 5, 5)$, $(5, -5, 5)$, and $(5, 5, -5)$.

Table 8
Scattering of a spherical wave (3) with $x_0 = (5, -5, 5)$.

Grid	h	$k = 1$, $\{L_q\} = \{19, 11, 11\}$		$k = 5$, $\{L_q\} = \{23, 17, 15\}$		$k = 10$, $\{L_q\} = \{31, 23, 21\}$	
		$\|u^{(h)} - u^{(2h)}\|_\infty$	Rate	$\|u^{(h)} - u^{(2h)}\|_\infty$	Rate	$\|u^{(h)} - u^{(2h)}\|_\infty$	Rate
64	0.088	$9.7450 \cdot 10^{-4}$	–	$1.3241 \cdot 10^{-1}$	–	$2.4335 \cdot 10^{-1}$	–
128	0.044	$1.7645 \cdot 10^{-5}$	5.78	$1.5893 \cdot 10^{-4}$	9.70	$1.0569 \cdot 10^{-3}$	7.84
256	0.022	$8.6687 \cdot 10^{-8}$	7.66	$1.4670 \cdot 10^{-6}$	6.75	$8.1193 \cdot 10^{-6}$	7.02
512	0.011	$9.5312 \cdot 10^{-10}$	6.50	$9.1998 \cdot 10^{-9}$	7.31	$7.5340 \cdot 10^{-8}$	6.75

Table 9
Scattering of a spherical wave (3) with $x_0 = (5, 5, -5)$.

Grid	h	$k = 1$, $\{L_q\} = \{19, 11, 11\}$		$k = 5$, $\{L_q\} = \{31, 17, 15\}$		$k = 10$, $\{L_q\} = \{31, 23, 21\}$	
		$\|u^{(h)} - u^{(2h)}\|_\infty$	Rate	$\|u^{(h)} - u^{(2h)}\|_\infty$	Rate	$\|u^{(h)} - u^{(2h)}\|_\infty$	Rate
64	0.088	$1.0565 \cdot 10^{-3}$	–	$1.3241 \cdot 10^{-1}$	–	$2.4335 \cdot 10^{-1}$	–
128	0.044	$1.7319 \cdot 10^{-5}$	5.93	$1.5893 \cdot 10^{-4}$	9.70	$1.0569 \cdot 10^{-3}$	7.84
256	0.022	$8.5229 \cdot 10^{-8}$	7.66	$1.4670 \cdot 10^{-6}$	6.75	$8.1193 \cdot 10^{-6}$	7.02
512	0.011	$2.6097 \cdot 10^{-9}$	5.02	$9.1998 \cdot 10^{-9}$	7.31	$7.5340 \cdot 10^{-8}$	6.75

5. Discussion

We used the method of difference potentials combined with a sixth order accurate compact finite difference scheme and high order Bayliss–Gunzburger–Turkel absorbing boundary conditions to simulate constant coefficient 3D wave scattering about multiple non-conforming spherical obstacles using only regular Cartesian grids. Our computations confirm the design sixth order accuracy of the method.

The MDP involves neither auxiliary variables nor singular integrals. It automatically translates the well-posedness of the original problem to its equivalent boundary formulation. This is in contrast to the approach based on boundary integral equations (BIEs), where one needs to carefully choose a proper representation of the solution (e.g., a single-layer or double-layer potential) to get a well-posed integral equation (Fredholm second kind). This task may become nontrivial when different boundary conditions are set on different parts of the boundary, e.g., different scatterers. Furthermore, the difference potentials approach can be generalized to the time dependent wave equation [37,40], which is difficult for the integral equations approach.

Yet another important distinction from the BIEs is that our results can be extended to a variable speed of sound (inside the artificial outer boundary). In two space dimensions, that was done in our previous work [32–34]. In BIEs, this is not possible because converting the Helmholtz equation to an integral equation over the surface requires knowledge of the Green's function for the Helmholtz equation. For a general spatially dependent speed of sound, it is not known. Our method, on the other hand, can accommodate a variable propagation speed. This requires a modified compact sixth order finite difference scheme and extension operator. The equation-based differentiation would also need to be modified accordingly. All these modifications have already been done in other applications. A major change would be the necessity to replace the direct solver based on the separation of variables and FFT by an iterative solver for the auxiliary problem. Indeed, when solving the AP one must invert a large nonsymmetric and nonpositive matrix and if the propagation speed varies the FFT does not apply. As the same AP needs to be solved repeatedly for different right-hand sides, one can employ a direct solver that would be particularly efficient in this situation, for example, PARDISO [41]. However, in three dimensions and when the domain is many wavelengths in size, no direct solver other than the FFT is likely to be feasible even on modern computers. Hence, an iterative method presents the only way forward.

Originally, standard Krylov techniques, such as GMRES or BiCGSTAB, were used frequently for solving the Helmholtz equation, supplemented by algebraic preconditioners (such as incomplete LU). In recent years, several other approaches have been introduced. Gordon and Gordon [42] used a variant of the Kaczmarz algorithm, named CARP-CG, that can be parallelized. Its interesting feature is that it becomes more efficient as the wave number becomes larger, i.e. the matrix departs further from diagonal dominance. Bayliss, Goldstein, and Turkel [43] used a preconditioner based on the Laplace operator. That was extended by Erlangga, et al. in a series of papers [44–47] to use a Helmholtz equation with a complex wavenumber, which can be solved efficiently, in particular, by multigrid. Engquist and Ying [48,49] introduced an efficient sweeping method to solve the system of equations originating from a discretization of the Helmholtz equation. Tal-Ezer and Turkel [50] presented an iterative solver that proves particularly efficient for multiple right-hand sides. This is advantageous for our algorithm as it requires solving the same AP for different right-hand sides.

Another approach is domain decomposition (see, e.g., [51–53]), where the subdomains can be either overlapping or non-overlapping. Non-overlapping domain decomposition methods (DDMs) attempt to alleviate the cost growth of solving the Helmholtz equation on large domains by breaking the domain down into smaller, simpler subdomains thus creating subproblems that are coupled to one another along their interfaces. Traditionally, DDMs resolve this coupling by an iterative process that alternates between directly solving a localized approximation of the subproblem and updating the resulting boundary conditions using parameterized transmission conditions. The convergence rate of the iterative process

is heavily dependent on the transmission conditions, the choice of which is a highly active research area (see, e.g., [54–61]). Recently, Gander and Zhang [62] presented a survey of many modern techniques to iteratively solve the Helmholtz equation even with a variable speed of sound. In [63], we have developed a non-overlapping domain decomposition using the method of difference potentials.

Let us also re-iterate that, the difference potentials approach requires only simple meshes such as Cartesian or spherical. In contrast, a finite element method requires grid generation which is nontrivial for a domain with many generally shaped scatterers in three space dimensions.

Our future work on multiple scattering will include improving the efficiency by replacing the global approach with a new one in which each obstacle is solved independently with transfer operators for each subdomain that couple the various regions. This can be thought of as domain decomposition where the individual subdomains have no common interfaces; they are rather separated in space and the connections between them are rendered by the transmission operators. Such an approach was used by Grote and Kirsch [12] using DtN as the nonreflecting boundary condition coupled with a second order finite difference scheme in polar coordinates for each scatterer. However, unlike our current approach that surrounds all scatterers with one common artificial outer boundary and can be modified to handle the variable propagation speed inside the computational domain, the transfer operators needed for decomposition inherently rely on constant coefficients in-between the scatterers. Previous work with similar approaches include Acosta and Villamizar [13], Min and Kim [14] and Jiang and Zheng [15] who have used second order finite element codes for obstacles that conform with the grid.

Declaration of competing interest

The authors declare that they have no known competing financial interests or personal relationships that could have appeared to influence the work reported in this paper.

References

[1] Leung Tsang, Jin Au Kong, Kung-Hau Ding, Chi On Ao, Scattering of Electromagnetic Waves: Numerical Simulations, John Wiley & Sons, Ltd, 2002.
[2] John D. Joannopoulos, Steven G. Johnson, Joshua N. Winn, Robert D. Meade, Photonic Crystals: Molding the Flow of Light, second ed., Princeton University Press, 2008.
[3] Diederik S. Wiersma, Disordered photonics, Nat. Photonics 7 (2013) 188–196.
[4] Matthias Ehrhardt (Ed.), Wave Propagation in Periodic Media, in: Progress in Computational Physics (PiCP), vol. 1, Bentham Science Publishers, 2010, Numerical techniques and practical applications.
[5] J. Coatléven, P. Joly, Operator factorization for multiple-scattering problems and an application to periodic media, Commun. Comput. Phys. 11 (2) (2012) 303–318.
[6] P.A. Martin, Multiple Scattering, in: Encyclopedia of Mathematics and its Applications, vol. 107, Cambridge University Press, Cambridge, 2006, Interaction of time-harmonic waves with *N* obstacles.
[7] Xavier Antoine, Marion Darbas, Integral equations and iterative schemes for acoustic scattering problems, in: F. Magoulès (Ed.), Numerical Methods for Acoustics Problems, Saxe-Coburg Editors, 2016.
[8] David Colton, Rainer Kress, Inverse Acoustic and Electromagnetic Scattering Theory, second ed., in: Applied Mathematical Sciences, vol. 93, Springer-Verlag, Berlin, 1998.
[9] Jean-Claude Nédélec, Acoustic and Electromagnetic Equations, in: Applied Mathematical Sciences, vol. 144, Springer-Verlag, New York, 2001, Integral representations for harmonic problems.
[10] Eli Turkel, Dan Gordon, Rachel Gordon, Semyon Tsynkov, Compact 2D and 3D sixth order schemes for the Helmholtz equation with variable wave number, J. Comput. Phys. 232 (1) (2013) 272–287.
[11] V.S. Ryaben'kii, Method of Difference Potentials and its Applications, in: Springer Series in Computational Mathematics, vol. 30, Springer-Verlag, Berlin, 2002.
[12] Marcus J. Grote, Christoph Kirsch, Dirichlet-to-Neumann boundary conditions for multiple scattering problems, J. Comput. Phys. 201 (2) (2004) 630–650.
[13] Sebastian Acosta, Vianey Villamizar, Coupling of Dirichlet-to-Neumann boundary condition and finite difference methods in curvilinear coordinates for multiple scattering, J. Comput. Phys. 229 (15) (2010) 5498–5517.
[14] Youngho Min, Seungil Kim, Dirichlet-to-Neumann boundary conditions for multiple scattering in waveguides, Comput. Math. Appl. 79 (6) (2020) 1661–1686.
[15] Xue Jiang, Weiying Zheng, Adaptive perfectly matched layer method for multiple scattering problems, Comput. Methods Appl. Mech. Engrg. 201–204 (2012) 42–52.
[16] Sebastian Acosta, On-surface radiation condition for multiple scattering of waves, Comput. Methods Appl. Mech. Engrg. 283 (2015) 1296–1309.
[17] Sebastian Acosta, Local on-surface radiation condition for multiple scattering of waves from convex obstacles, 2019, arXiv:1911.01513.
[18] Hasan Alzubaidi, Xavier Antoine, Chokri Chniti, Formulation and accuracy of on-surface radiation conditions for acoustic multiple scattering problems, Appl. Math. Comput. 277 (2016) 82–100.
[19] Marcus J. Grote, Imbo Sim, Local nonreflecting boundary condition for time-dependent multiple scattering, J. Comput. Phys. 230 (8) (2011) 3135–3154.
[20] Alvin Bayliss, Eli Turkel, Radiation boundary conditions for wave-like equations, Comm. Pure Appl. Math. 33 (6) (1980) 707–725.
[21] Thomas Hagstrom, S.I. Hariharan, A formulation of asymptotic and exact boundary conditions using local operators, Appl. Numer. Math. 27 (4) (1998) 403–416, Absorbing boundary conditions.
[22] Alvin Bayliss, Max Gunzburger, Eli Turkel, Boundary conditions for the numerical solution of elliptic equations in exterior regions, SIAM J. Appl. Math. 42 (2) (1982) 430–451.
[23] M. Medvinsky, S. Tsynkov, E. Turkel, Direct implementation of high order BGT artificial boundary conditions, J. Comput. Phys. 376 (2019) 98–128.

[24] M. Medvinsky, S. Tsynkov, E. Turkel, Solving the Helmholtz equation for general smooth geometry using simple grids, Wave Motion 62 (2016) 75–97.
[25] A.P. Calderon, Boundary-value problems for elliptic equations, in: Proceedings of the Soviet-American Conference on Partial Differential Equations in Novosibirsk, Fizmatgiz, Moscow, 1963, pp. 303–304.
[26] R.T. Seeley, Singular integrals and boundary value problems, Amer. J. Math. 88 (1966) 781–809.
[27] Eli Turkel, Dan Gordon, Rachel Gordon, Semyon Tsynkov, Compact 2D and 3D sixth order schemes for the Helmholtz equation with variable wave number, J. Comput. Phys. 232 (1) (2013) 272–287.
[28] A.N. Tikhonov, A.A. Samarskii, Equations of Mathematical Physics, Dover Publications, Inc., New York, 1990, Translated from the Russian by A. R. M. Robson and P. Basu, Reprint of the 1963 translation.
[29] Philip M. Morse, Herman Feshbach, Methods of Theoretical Physics. 2 Volumes, in: International Series in Pure and Applied Physics, McGraw-Hill Book Co. Inc., New York, 1953.
[30] A.A. Reznik, Approximation of surface potentials of elliptic operators by difference potentials, Soviet Math. Dokl. 25 (2) (1982) 543–545.
[31] A.A. Reznik, Approximation of the Surface Potentials of Elliptic Operators by Difference Potentials and Solution of Boundary-Value Problems (Ph.D. thesis), Moscow Institute for Physics and Technology, Moscow, USSR, 1983, [in Russian].
[32] M. Medvinsky, S. Tsynkov, E. Turkel, The method of difference potentials for the Helmholtz equation using compact high order schemes, J. Sci. Comput. 53 (1) (2012) 150–193.
[33] D.S. Britt, S.V. Tsynkov, E. Turkel, A high-order numerical method for the Helmholtz equation with nonstandard boundary conditions, SIAM J. Sci. Comput. 35 (5) (2013) A2255–A2292.
[34] M. Medvinsky, S. Tsynkov, E. Turkel, High order numerical simulation of the transmission and scattering of waves using the method of difference potentials, J. Comput. Phys. 243 (2013) 305–322.
[35] Michael Medvinsky, Michael Medvinsky High Order Numerical Simulation of Waves using Regular Grids and Non-Conforming Interfaces (Ph.D. thesis), Tel Aviv University, 2013.
[36] D.S. Britt, S.V. Tsynkov, E. Turkel, A high-order numerical method for the Helmholtz equation with nonstandard boundary conditions, SIAM J. Sci. Comput. 35 (5) (2013) A2255–A2292.
[37] S. Petropavlovsky, S. Tsynkov, E. Turkel, A method of boundary equations for unsteady hyperbolic problems in 3D, J. Comput. Phys. 365 (2018) 294–323.
[38] Sven Hammarling, Craig Lucas, Updating the QR Factorization and the Least Squares Problem. MIMS EPrint 2008.111, Manchester Institute for Mathematical Sciences, School of Mathematics, University of Manchester, 2008.
[39] A. Bayliss, C.I. Goldstein, E. Turkel, On accuracy conditions for the numerical computation of waves, J. Comput. Phys. 59 (3) (1985) 396–404.
[40] Sergey Petropavlovsky, Semyon V. Tsynkov, Eli Turkel, Numerical solution of 3D exterior unsteady wave propagation problems using boundary operators, SIAM J. Sci. Comput. 42 (5) (2020) A3462–A3488.
[41] https://www.pardiso-project.org.
[42] Dan Gordon, Rachel Gordon, Robust and highly scalable parallel solution of the Helmholtz equation with large wave numbers, J. Comput. Appl. Math. 237 (1) (2013) 182–196.
[43] Alvin Bayliss, Charles I. Goldstein, Eli Turkel, An iterative method for the Helmholtz equation, J. Comput. Phys. 49 (3) (1983) 443–457.
[44] Y.A. Erlangga, C. Vuik, C.W. Oosterlee, On a class of preconditioners for solving the Helmholtz equation, Appl. Numer. Math. 50 (3–4) (2004) 409–425.
[45] Yogi A. Erlangga, Cornelis Vuik, Cornelis W. Oosterlee, On a robust iterative method for heterogeneous Helmholtz problems for geophysics applications, Int. J. Numer. Anal. Model. 2 (suppl.) (2005) 197–208.
[46] Y.A. Erlangga, C.W. Oosterlee, C. Vuik, A novel multigrid based preconditioner for heterogeneous Helmholtz problems, SIAM J. Sci. Comput. 27 (4) (2006) 1471–1492, (electronic).
[47] Y.A. Erlangga, C. Vuik, C.W. Oosterlee, Comparison of multigrid and incomplete LU shifted-Laplace preconditioners for the inhomogeneous Helmholtz equation, Appl. Numer. Math. 56 (5) (2006) 648–666.
[48] Björn Engquist, Lexing Ying, Sweeping preconditioner for the Helmholtz equation: moving perfectly matched layers, Multiscale Model. Simul. 9 (2) (2011) 686–710.
[49] Björn Engquist, Lexing Ying, Sweeping preconditioner for the Helmholtz equation: hierarchical matrix representation, Comm. Pure Appl. Math. 64 (5) (2011) 697–735.
[50] Hillel Tal-Ezer, Eli Turkel, The iterative solver Risolv with application to the exterior Helmholtz problem, SIAM J. Sci. Comput. 32 (1) (2010) 463–475.
[51] Alfio Quarteroni, Alberto Valli, Domain decomposition methods for partial differential equations, in: Numerical Mathematics and Scientific Computation, The Clarendon Press, Oxford University Press, New York, 1999, Oxford Science Publications.
[52] F. Nataf, F. Nier, Convergence rate of some domain decomposition methods for overlapping and nonoverlapping subdomains, Numer. Math. 75 (3) (1997) 357–377.
[53] Victorita Dolean, Pierre Jolivet, Frédéric Nataf, An Introduction to Domain Decomposition Methods, Society for Industrial and Applied Mathematics (SIAM), Philadelphia, PA, 2015, Algorithms, theory, and parallel implementation..
[54] Y. Boubendir, X. Antoine, C. Geuzaine, A quasi-optimal non-overlapping domain decomposition algorithm for the Helmholtz equation, J. Comput. Phys. 231 (2) (2012) 262–280.
[55] Christiaan C. Stolk, A rapidly converging domain decomposition method for the Helmholtz equation, J. Comput. Phys. 241 (2013) 240–252.
[56] Yassine Boubendir, Dawid Midura, Non-overlapping domain decomposition algorithm based on modified transmission conditions for the Helmholtz equation, Comput. Math. Appl. 75 (6) (2018) 1900–1911.
[57] V. Mattesi, M. Darbas, C. Geuzaine, A high-order absorbing boundary condition for 2D time-harmonic elastodynamic scattering problems, Comput. Math. Appl. 77 (6) (2019) 1703–1721.
[58] A. Modave, A. Royer, X. Antoine, C. Geuzaine, A non-overlapping domain decomposition method with high-order transmission conditions and cross-point treatment for Helmholtz problems, Comput. Methods Appl. Mech. Engrg. 368 (2020) 113162, 23.
[59] Dan Gordon, Rachel Gordon, CADD: A seamless solution to the domain decomposition problem of subdomain boundaries and cross-points, Wave Motion 98 (2020) 102649, (11pp).
[60] Francis Collino, Patrick Joly, Matthieu Lecouvez, Exponentially convergent non overlapping domain decomposition methods for the Helmholtz equation, ESAIM Math. Model. Numer. Anal. 54 (3) (2020) 775–810.
[61] Ruiyang Dai, Axel Modave, Jean-Francois Remacle, Christophe Geuzaine, Multidirectionnal sweeping preconditioners with non-overlapping checkerboard domain decomposition for Helmholtz problems, 2021.
[62] Martin J. Gander, Hui Zhang, A class of iterative solvers for the Helmholtz equation: factorizations, sweeping preconditioners, source transfer, single layer potentials, polarized traces, and optimized Schwarz methods, SIAM Rev. 61 (1) (2019) 3–76.
[63] Evan North, Semyon Tsynkov, Eli Turkel, Non-iterative domain decomposition for the Helmholtz equation with strong material discontinuities, Appl. Numer. Math. (2021) submitted for publication.